Enhancing V_{S30} Mapping in the Taipei Basin: Integrating New V_S Estimation Functions, Extrapolated V_S Profiles, and Kriging with Varying Local Means

Stefan C. Nicholas[1], Linh Thi Mai Nguyen[1], Chun-Liang Kuo[1], Jia-Cian Gao[1,2,3], Chun-Hsiang Kuo*[2,4,5], Duc-Huy Tran[1], Shih-Jung Wang[1], and Jia-Jyun Dong[1,2,4,6]

ABSTRACT

Taiwan is one of the most seismically active countries in the world, and the Taipei basin is particularly susceptible to earthquake hazards due to its high population density and local geology. Site effects, caused by soft sediment deposits overlying hard rock, amplify seismic waves and intensify seismic ground motion, posing significant challenges for seismic hazard assessments in the Taipei basin. To represent site effects, the average shear-wave velocity of the upper 30 m (V_{S30}) is commonly used. However, direct V_S measurements are relatively scarce compared to the abundance of engineering boreholes, which often include soil parameters such as void ratio and unit weight. This study proposes new estimation functions that correlate these parameters with V_S, enabling the inference of V_S at borehole locations without direct measurements. This study also builds upon previous research by incorporating a larger and more comprehensive database, made possible by the availability of additional data and the extrapolation of V_S profiles from shallow boreholes (less than 30 m in depth). In addition, we employed Kriging with varying local means to generate a V_{S30} distribution map across the Taipei basin. The results indicate that the V_{S30} distribution in the Taipei basin ranges from ~150–600 m/s, with some areas in the northern part of the basin identified as having lower V_{S30}-values (< 180 m/s), which may result in amplified ground motion. Compared with previous research, our study significantly enhances the spatial coverage and resolution of V_{S30} mapping in the Taipei basin, providing valuable insights for assessing seismic hazard.

KEY POINTS

- A high-resolution V_{S30} map is developed for the Taipei basin, a seismically vulnerable region.
- V_{S30} estimates are improved using new V_S estimation functions, extrapolated V_S profiles, and a Kriging method.
- The approach enhances V_{S30}-based site characterization and supports seismic hazard assessment in the basin.

Supplemental Material

INTRODUCTION

Taiwan frequently experiences earthquakes, posing threats to human life and property, with their intensity strongly influenced by site effects that depend on geological and topographical conditions (Gutenberg, 1957). The Taipei basin is particularly vulnerable due to the combination of soft alluvial sediment overlying bedrock and its topographic setting, which enhances site effects by amplifying seismic waves and prolonging ground shaking (Kuo *et al.*, 2011). One commonly used parameter for assessing site effects is the time-averaged shear-wave velocity within the top 30 m of the ground (V_{S30}; Building Seismic Safety Council [BSSC], 1995; Anderson *et al.*, 1996; Park and Elrick, 1998; Huang *et al.*, 2007). Although V_{S30} is not a physical

1. Graduate Institute of Applied Geology, National Central University, Taoyuan, Taiwan, https://orcid.org/0009-0003-6537-4505 (LTMN); https://orcid.org/0009-0005-6325-7414 (C-LK); https://orcid.org/0000-0001-7870-8496 (D-HT); https://orcid.org/0000-0002-7616-2343 (S-JW); https://orcid.org/0000-0003-4287-7719 (J-JD); 2. Earthquake-Disaster and Risk Evaluation and Management Center, National Central University, Taoyuan, Taiwan, https://orcid.org/0000-0003-4602-385X (C-HK); 3. Graduate College of Sustainability and Green Energy, National Central University, Taoyuan, Taiwan; 4. Department of Earth Sciences, National Central University, Taoyuan, Taiwan; 5. National Center for Research on Earthquake Engineering, Taipei, Taiwan; 6. Center for Environmental Studies, National Central University, Taoyuan, Taiwan

*Corresponding author: chkuo@ncu.edu.tw

Cite this article as Nicholas, S. C., L. T. M. Nguyen, C.-L. Kuo, J.-C. Gao, C.-H. Kuo, D.-H. Tran, S.-J. Wang, and J.-J. Dong (2025). Enhancing V_{S30} Mapping in the Taipei Basin: Integrating New V_S Estimation Functions, Extrapolated V_S Profiles, and Kriging with Varying Local Means, *Bull. Seismol. Soc. Am.* **115**, 2439–2463, doi: 10.1785/0120250020

© Seismological Society of America

Downloaded from http://pubs.geoscienceworld.org/ssa/bssa/article-pdf/115/5/2439/7295436/bssa-2025020.1.pdf by National Central Univ Library Serials Office user on 08 December 2025

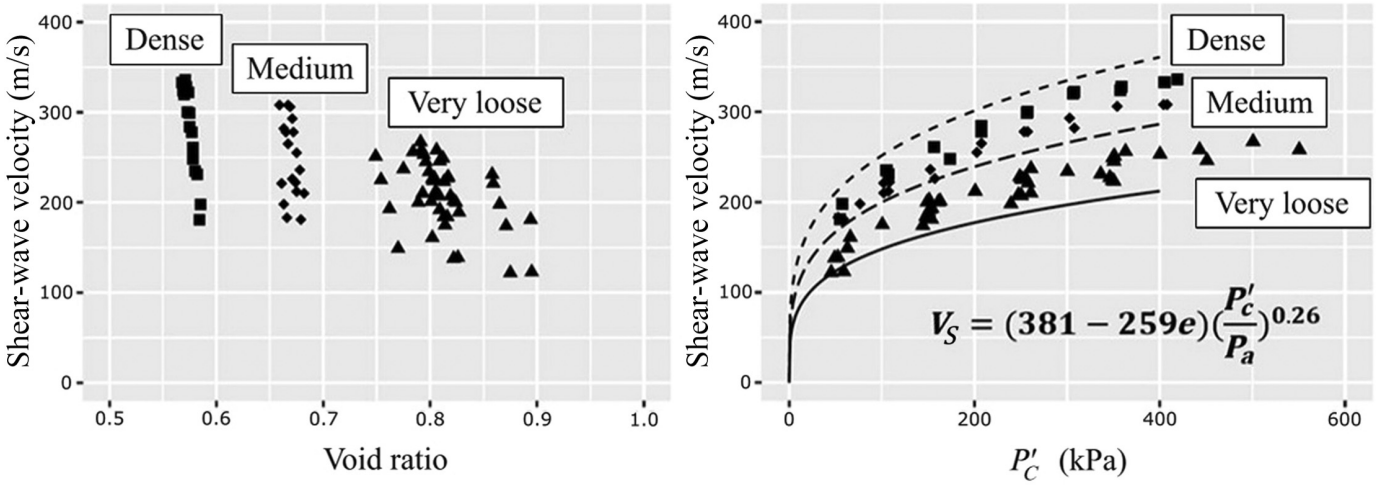

Figure 1. Relationship among void ratio, average effective stress (P_c'), and shear-wave velocity. The regression equation includes a constant value for atmospheric pressure (P_a = 100 kPa). This figure is modified from Robertson *et al.* (1995).

parameter of site amplification (Ahdi *et al.*, 2022; Kuo and Abrahamson, 2023), it serves as a useful proxy due to its empirical correlation with deeper velocity structures, which influence seismic response (Boore *et al.*, 2011). However, although V_{S30} is widely used due to its correlation with site amplification, it has limitations as a single-parameter proxy because it does not capture full depth-dependent variations in V_S, velocity impedance, or 2D/3D site effects. Nonetheless, this study utilizes V_{S30} primarily for its practicality because it can be estimated from engineering boreholes, which are far more abundant than deep V_S profiles. This makes it a universally applicable parameter for regional-scale hazard assessments. In recent years, developing accurate V_{S30} maps for various regions has gained significant attention (Kim and Hong, 2022; Xie *et al.*, 2022; Zhang *et al.*, 2023) because regional V_{S30} mapping is critical for site-specific hazard assessments. Recent approaches to V_{S30} mapping mostly involve a combination of geophysical surveys, geological investigations, and empirical models (Ahdi *et al.*, 2022; Zhang *et al.*, 2023). However, these approaches can have significant uncertainties due to low borehole densities, insufficient data, and inconsistent empirical equations. In addition, the uncertainty associated with predicted V_{S30}-values compared to measured V_{S30} can be considerably higher, highlighting the need for accurate V_{S30} estimation (Chao *et al.*, 2021).

The Taipei basin is selected as the study region, due to the large amount of both deep and shallow borehole data available and the importance of site-specific seismic hazard assessments for this area. Despite the Taipei basin's depth exceeding 30 m, V_{S30} is critical for seismic design codes in Taiwan. Previous studies have explored various approaches to estimate V_{S30} in Taiwan and the Taipei basin. These approaches can be categorized as directly estimating V_{S30} using geological or topographic data, or first estimating the shear-wave velocity (V_S) of the subsurface stratigraphy and then using empirical formulas to estimate V_{S30}. The former approaches have employed proxies such as terrain slope, as demonstrated by Allen and Wald (2009), or hybrid models based on surface geology, terrain slope, and elevation, as developed by Kwok *et al.* (2018). Although the latter approaches use empirical formulas, which estimate V_S based on soil parameters such as the standard penetration test (SPT-N) values and/or depth, followed by the estimation of V_{S30} using drilling data (Lee and Tsai, 2008; Kuo *et al.*, 2011, 2012; Tsai *et al.*, 2019). However, SPT-N values may introduce high uncertainty due to equipment limitations and potential human error. Similarly, correlations based on cone penetration test (CPT) data can be influenced by variations in soil behavior, equipment sensitivity, and site-specific factors, leading to additional uncertainties. Therefore, it is necessary to explore alternative approaches to establish more accurate empirical equations that relate soil parameters to V_S.

This study aims to enhance V_{S30} estimation in the Taipei basin by developing improved estimation functions based on the correlations between shear-wave velocity, void ratio (e), and effective stress (σ'). These estimation functions are empirical models that predict V_S by statistically relating it to physical soil parameters (e, σ'). Figure 1, adapted from Robertson *et al.* (1995), illustrates the empirical relationship between e, σ', and V_S, which serves as the foundational basis for our V_S estimation functions. Although void ratio or effective stress alone can correspond to a relatively wide range of V_S-values, using both parameters together is expected to yield more consistent estimates by accounting for their combined influence. These functions are particularly useful in contexts in which direct V_S measurements are sparse, but geotechnical parameters are available from abundant engineering boreholes, which is a common scenario in many regions worldwide. Although void ratio and effective stress are derived from disturbed samples, their use provides a more direct physical basis for estimating

Downloaded from http://pubs.geoscienceworld.org/ssa/bssa/article-pdf/115/5/2439/7295436/bssa-2025020.1.pdf by National Central Univ Library Serials Office user on 08 December 2025

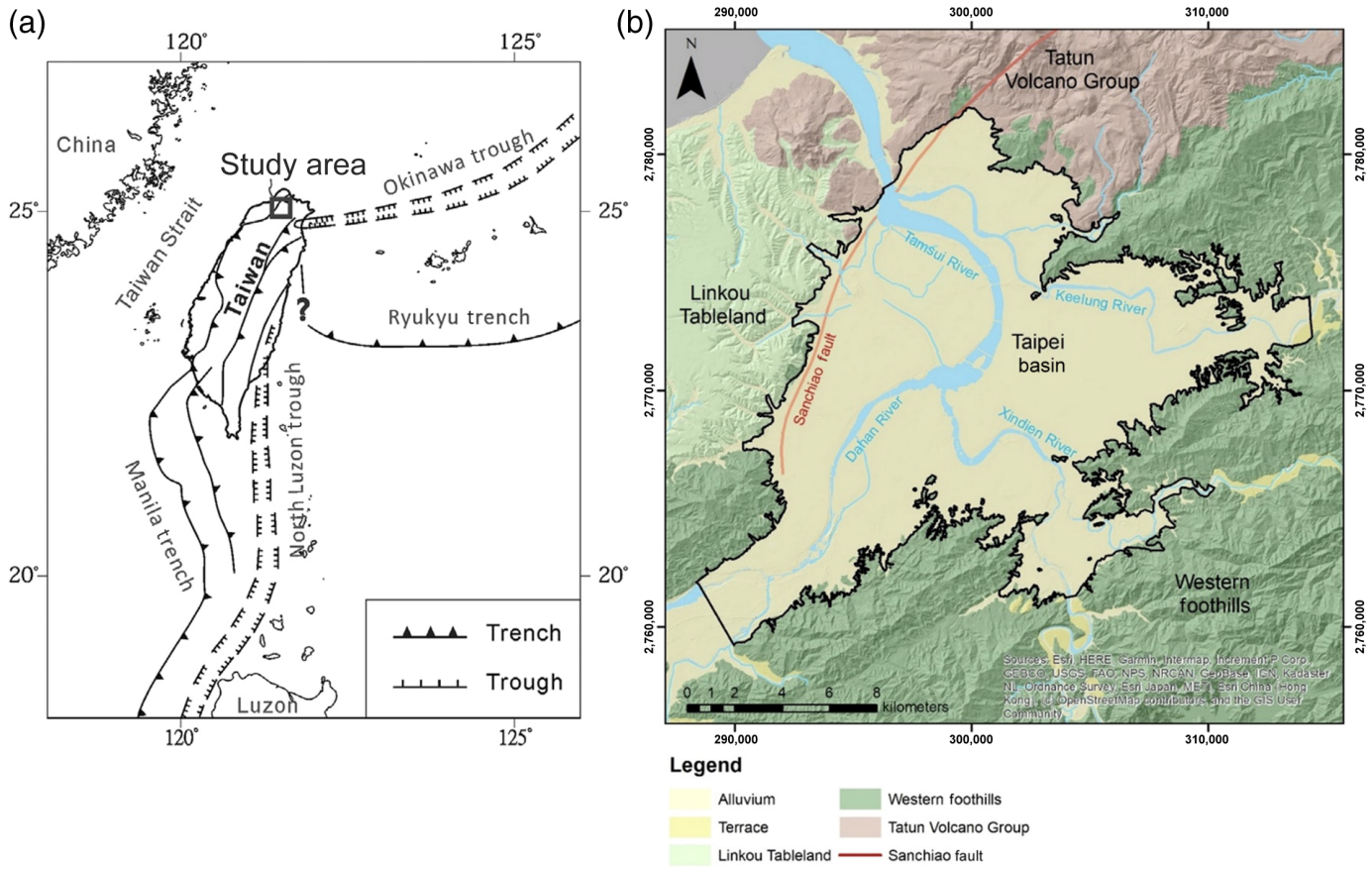

Figure 2. (a) Tectonic setting of Taiwan (from Su *et al.*, 2018). (b) Geological provinces within the Taipei basin area (modified from Su *et al.*, 2018). The black line outlines the extent of the Taipei basin. The color version of this figure is available only in the electronic edition.

V_S than empirical correlations based on SPT or CPT data. The influence of the inherent uncertainty from geotechnical parameters derived from disturbed samples on V_S estimation is quantified in the Discussion section.

Two databases are utilized in this study: the Engineering Geological Database for Taiwan Strong Motion Instrumentation Program (EGDT), which includes directly measured V_S by a suspension *PS*-logging system and geotechnical logging data (Kuo *et al.*, 2012), and the Central Geological Survey (CGS) database, which provides geotechnical data from boreholes, but without V_S information (see Data and Resources). In addition, this study seeks to expand the CGS database by extrapolating shallow borehole data (boreholes less than 30 m in depth), which significantly increases the amount of data available for spatial interpolation of V_{S30} in the Taipei basin. This research compares three extrapolation techniques: the bottom constant velocity (BCV) model, the conditional independent property (CIP) model, and the model proposed by Boore *et al.* (2011), to determine the most accurate method for predicting V_{S30} from shallow boreholes within the Taipei basin. Furthermore, this study uses Kriging with varying local means for the spatial interpolation of V_{S30}. The research process can be divided into four main parts: (1) development of V_S estimation functions; (2) calculation of V_{S30}; (3) extrapolation of shallow V_S profiles to estimate V_{S30}; and (4) V_{S30} mapping using Kriging with varying local means.

STUDY AREA AND DATABASE

The Taipei basin

The Taipei basin, the primary focus area of this study, is located in the northeastern part of Taiwan, within the northern section of the western Foothills (Fig. 2). The basin's formation is primarily attributed to tectonic subsidence caused by flexural bending from the collision between the Philippine Sea plate and the Eurasian plate. The basin covers an area of about 243 km^2 and is bordered by the Linkou Tableland to the west, the Tatun Volcanic Complex to the north, and the western Foothills to the south and east. The Taipei basin predominantly consists of Quaternary sediments, including alluvial, fluvial, and estuarine deposits that have alternated with sea level fluctuations (Teng *et al.*, 2001). The depth of bedrock in the Taipei basin varies significantly, ranging from ∼−700 m in the western part of the basin due to subsidence along the Shanchiao fault and becoming progressively shallower toward the basin margins. The top 30 m of the ground, critical for evaluating site effects and V_{S30}, primarily consists of the Sungshan Formation, representing the shallowest and weakest

Downloaded from http://pubs.geoscienceworld.org/ssa/bssa/article-pdf/115/5/2439/7295436/bssa-2025020.1.pdf by National Central Univ Library Serials Office user on 08 December 2025

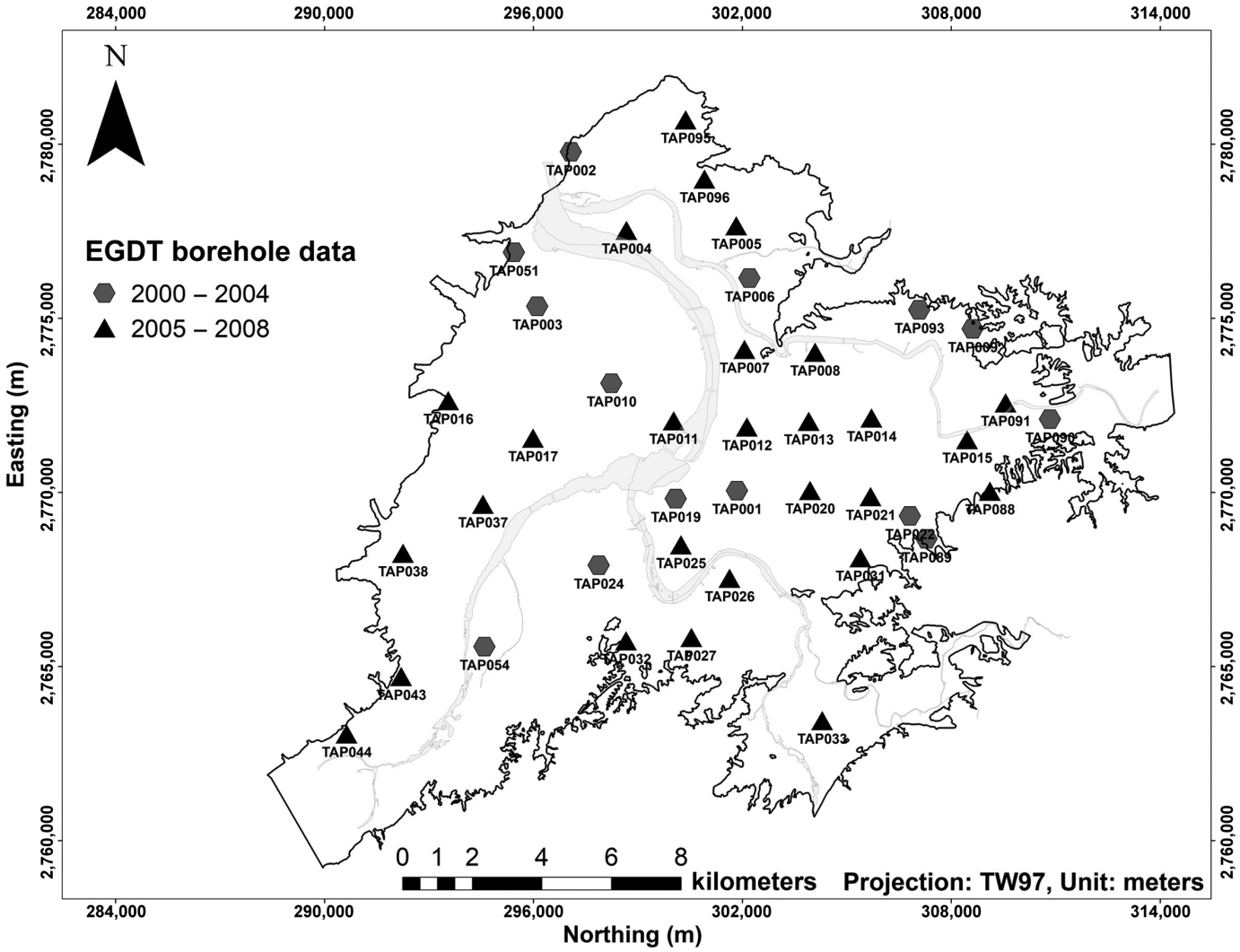

Figure 3. Map of the Taipei basin showing a total of 41 boreholes from the Engineering Geological Database for Taiwan Strong Motion Instrumentation Program (EGDT) database; 27 boreholes were utilized for regression analysis, whereas 14 boreholes were later excluded based on filter conditions.

alluvial deposits in the basin. This formation is characterized by fluvial to estuarine sands and muds (Huang, 1962; Peng *et al.*, 1999; Hong *et al.*, 2006), with occasional gravel deposits. Further inland, particularly toward the southern and eastern margins of the basin, the Jingmei Formation also occurs within the top 30 m. This formation consists of 20–40 m of alluvial fan gravel deposits (Teng *et al.*, 2000), likely resulting in higher V_{S30}-values in these areas.

EGDT

Since 2000, the Central Weather Bureau (CWB) and the National Center for Research on Earthquake Engineering (NCREE) have conducted a project to build the EGDT. This initiative aims to analyze the geological conditions at Taiwan's free-field strong-motion stations by conducting geological drilling and velocity measurements at various locations. Numerous previous studies have effectively utilized this database to establish shear-wave velocity regression equations (Lee and Tsai, 2008; Kuo *et al.*, 2012; Tsai *et al.*, 2019). The primary-wave velocity (V_P) and shear-wave velocity (V_S) measurements were taken using the OYO corporation's suspension *PS*-logging system. As part of the EGDT project, site investigations were carried out at 483 strong-motion stations across Taiwan from 2000 to 2019 (Kuo *et al.*, 2012), with data from all 41 stations located in the Taipei basin utilized for this study (Fig. 3). Because this database contains both direct V_S measurements and soil parameters such as e, and σ' derived from laboratory tests, it serves as the primary dataset for identifying correlations between V_S, e, and σ', enabling the development of V_S estimation functions for different soil types in our study. In addition, the measured V_S data will be used to compare different V_S extrapolation methods for shallow borehole data, and will serve as the primary variable for the V_{S30} map interpolation. However, before using these V_S measurements, a quality check was conducted to ensure their accuracy, as discussed in the

Downloaded from http://pubs.geoscienceworld.org/ssa/bssa/article-pdf/115/5/2439/7295436/bssa-2025020.1.pdf by National Central Univ Library Serials Office user on 08 December 2025

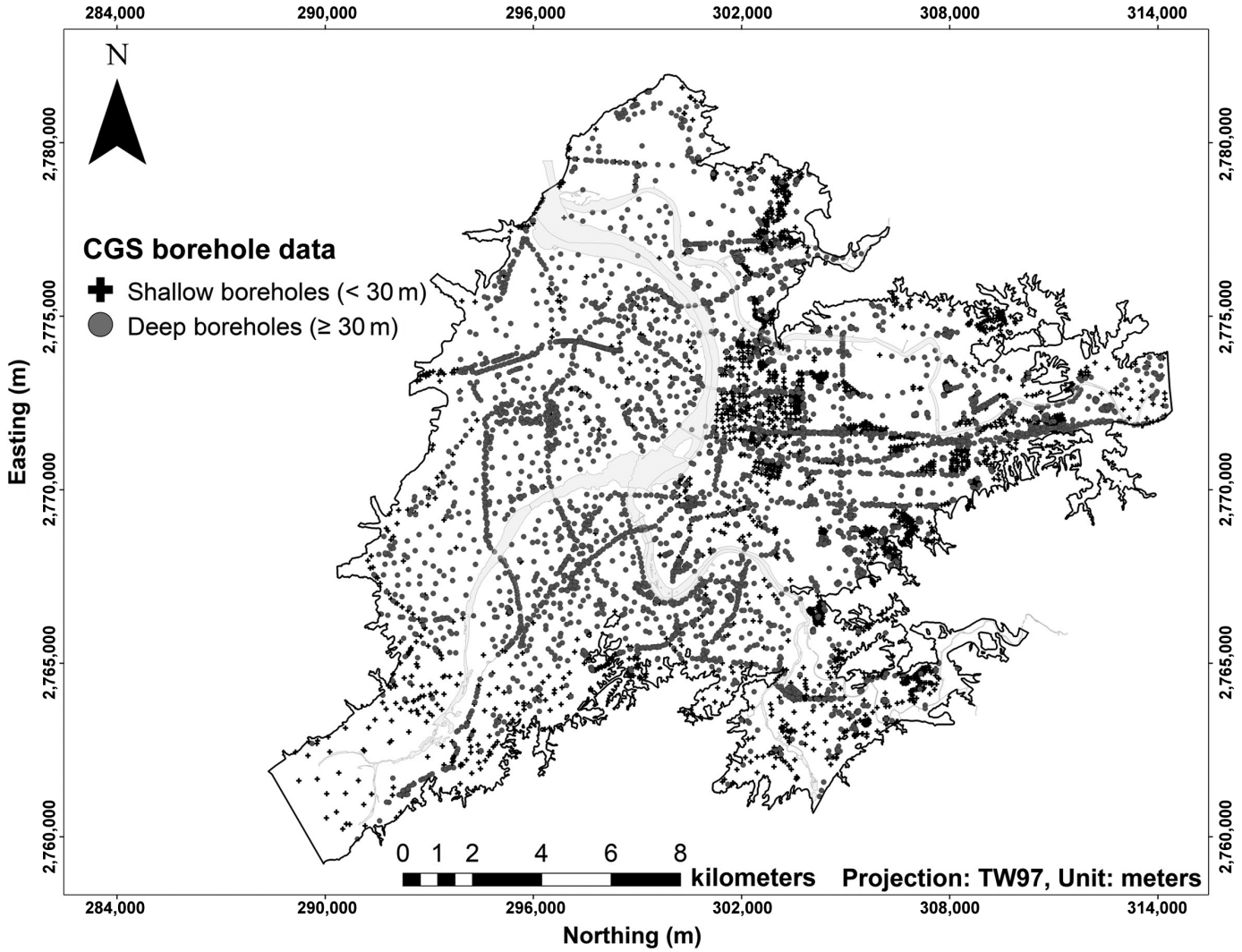

Figure 4. The distribution of 6766 Central Geological Survey (CGS) boreholes in the Taipei basin includes 2850 boreholes less than 30 m and 3916 boreholes equal to or greater than 30 m.

Methodology section. It is also important to note that soil parameters used in the V_S estimation functions were obtained from laboratory tests on disturbed samples, which may introduce uncertainty due to potential mismatch with in-situ conditions. This issue is acknowledged, and its implications are further discussed in the Methodology and Discussion sections.

CGS database

The CGS of the Ministry of Economic Affairs has initiated a project to collect engineering drilling data from various regions in Taiwan and compile it into a standardized format, creating an engineering geological exploration database. The primary objective of this initiative is to establish a centralized databank for the systematic recording and storage of geological information. Although the engineering drilling data from the Taipei basin primarily provide physical soil property test results without shear-wave velocity measurements, the extensive number of records offers an opportunity to improve V_{S30} data density. To achieve this, we apply the V_S estimation functions developed from the EGDT database, which correlate physical soil properties to V_S, enabling the estimation of shear-wave velocity in clay, silt, sand, and gravel. Although there are over 10,000 boreholes within the CGS database for the Taipei basin area, after a thorough data verification and screening process, 6,766 boreholes were selected for this study. The selection process involved two key steps: first, boreholes were filtered to include only those containing the required laboratory test data, such as void ratio and unit weight, necessary for the V_S estimation functions. Second, the remaining dataset was carefully examined to ensure data accuracy because some boreholes contained misclassified values, incorrect unit conversions, or misplaced data entries. Boreholes with such inconsistencies were either corrected or excluded from the final dataset. The location of the CGS boreholes is shown in Figure 4. Of the 6766 CGS boreholes used, 2850 had depths of less than 30 m and therefore required V_S-values to be extrapolated to 30 m to derive V_{S30}. All the estimated V_{S30}-

Downloaded from http://pubs.geoscienceworld.org/ssa/bssa/article-pdf/115/5/2439/7295436/bssa-2025020.1.pdf by National Central Univ Library Serials Office user on 08 December 2025

values from the CGS data were subsequently used as auxiliary variables for spatial interpolation using Kriging with varying local means to create the V_{S30} map.

METHODOLOGY

Shear-wave velocity estimation functions

Quality check of shear-wave velocity measurements. Before using the measured V_S-values from the EGDT database to perform the regression analysis required for developing the void ratio and effective stress-based V_S estimation functions, a V_S measurement quality check was conducted following an approach outlined by Lee and Tsai (2008). This method evaluates V_S measurement quality through both visual inspection and cross-correlation analysis. Although cross-correlation analysis assesses signal symmetry, visual inspection ensures the clarity of the initial waveform.

After these two criteria were checked, the measured V_S-values were then classified into two categories:

- High quality: clear first arrival, and the two traces from the opposite strikes are well correlated.
- Suboptimal: either the first arrival is unclear, the time lag between opposite tracks is excessively large, and/or significant correlation loss is present.

To develop the V_{S30} estimation functions in this study, only high-quality measurements were used to ensure reliability. However, during the Kriging with varying local means process, suboptimal V_S measurements were also included. Although lower in quality, these measurements still provide direct V_S observations and generally involve less uncertainty than predicted V_S. Furthermore, incorporating all direct V_S measurements helps capture local variations that might be overlooked by predicted V_S from estimation functions, which tend to provide more smoothed or averaged values.

Void ratio and vertical effective stress. Both void ratio (e) and vertical effective stress (σ_v') are closely related to V_S. Higher void ratios are often associated with looser, less dense soils that have more pore spaces. These soils typically exhibit lower stiffness, leading to lower V_S. Conversely, denser soils with lower void ratios tend to have higher V_S due to their higher stiffness and reduced pore space. Whereas higher vertical effective stress is typical in denser and stiffer soils, resulting in higher V_S. Although looser soils with lower stiffness generally have lower vertical effective stress, leading to lower V_S.

To develop the V_S estimation functions, laboratory test results for void ratio, water content, and unit weight were obtained from all 41 EGDT boreholes within the Taipei basin, providing 840 soil sample test results. However, some samples lacked recorded void ratio values. To address this, the void ratio for these samples was calculated using the following formula, based on standard soil mechanics principles (Craig, 2004):

$$e = \frac{(w+1) \times G_s \times \gamma_w - \gamma_t}{\gamma_t}, \tag{1}$$

in which w is the water content, G_s is the specific gravity, γ_w is the unit weight of water (9.807 kN/m^3), and γ_t is the unit weight of soil (kN/m^3).

To calculate vertical effective stress, pore pressure was first determined using a groundwater model that captured the total head (Fig. 5a). This model was developed using the Groundwater Modeling System (GMS) with MODFLOW, incorporating borehole lithology data and long-term groundwater observations. Vertical effective stress was then calculated using the following equation:

$$\sigma_v' = \Sigma(Z_i\gamma_i) - (h_p\gamma_w), \tag{2}$$

in which Z_i is the depth of each soil layer, h_p is the pressure head (total head–elevation), γ_i is the total unit weight of each soil layer, and γ_w is the unit weight of water.

However, because this model did not fully cover the entire basin, a simplified groundwater table trend surface (Fig. 5b) was applied in areas without total head data, particularly near the basin margins. For these locations, vertical effective stress was calculated using

$$\sigma_v' = \Sigma(Z_i\gamma_i) - [(Z_A - Z_W)\gamma_w], \tag{3}$$

in which Z_A is the borehole depth, and Z_W is the depth of the water table.

The choice of groundwater model is critical for this study because it influences the vertical effective stress, which in turn affects V_S estimates. Therefore, to assess the accuracy of both models, a validation test was conducted by comparing simulated groundwater levels to measured groundwater level data. The results showed that the total head model (GMS) had a lower root mean square error (rmse) (0.52 m) compared to the groundwater trend surface model (2.28 m). Consequently, the GMS model was used for most of the basin, whereas the trend surface model was applied only where total head data were unavailable. Further details of the groundwater models are provided in the supplemental material, available to this article. In addition, the uncertainty associated with variations in groundwater level and void ratio measurements on V_S and V_{S30} is reviewed in the Discussion section.

Pairing soil parameters with shear-wave velocity measurements. To establish the relationships between void ratio, effective stress, and V_S, the soil samples from EGDT boreholes were paired with V_S measurements from the same dataset. However, because soil samples and V_S measurements were recorded at different depth intervals, a matching procedure was required to form data pairs for regression analysis. Soil samples were collected at 1.5 m intervals with depth

Downloaded from http://pubs.geoscienceworld.org/ssa/bssa/article-pdf/115/5/2439/7295436/bssa-2025020.1.pdf by National Central Univ Library Serials Office user on 08 December 2025

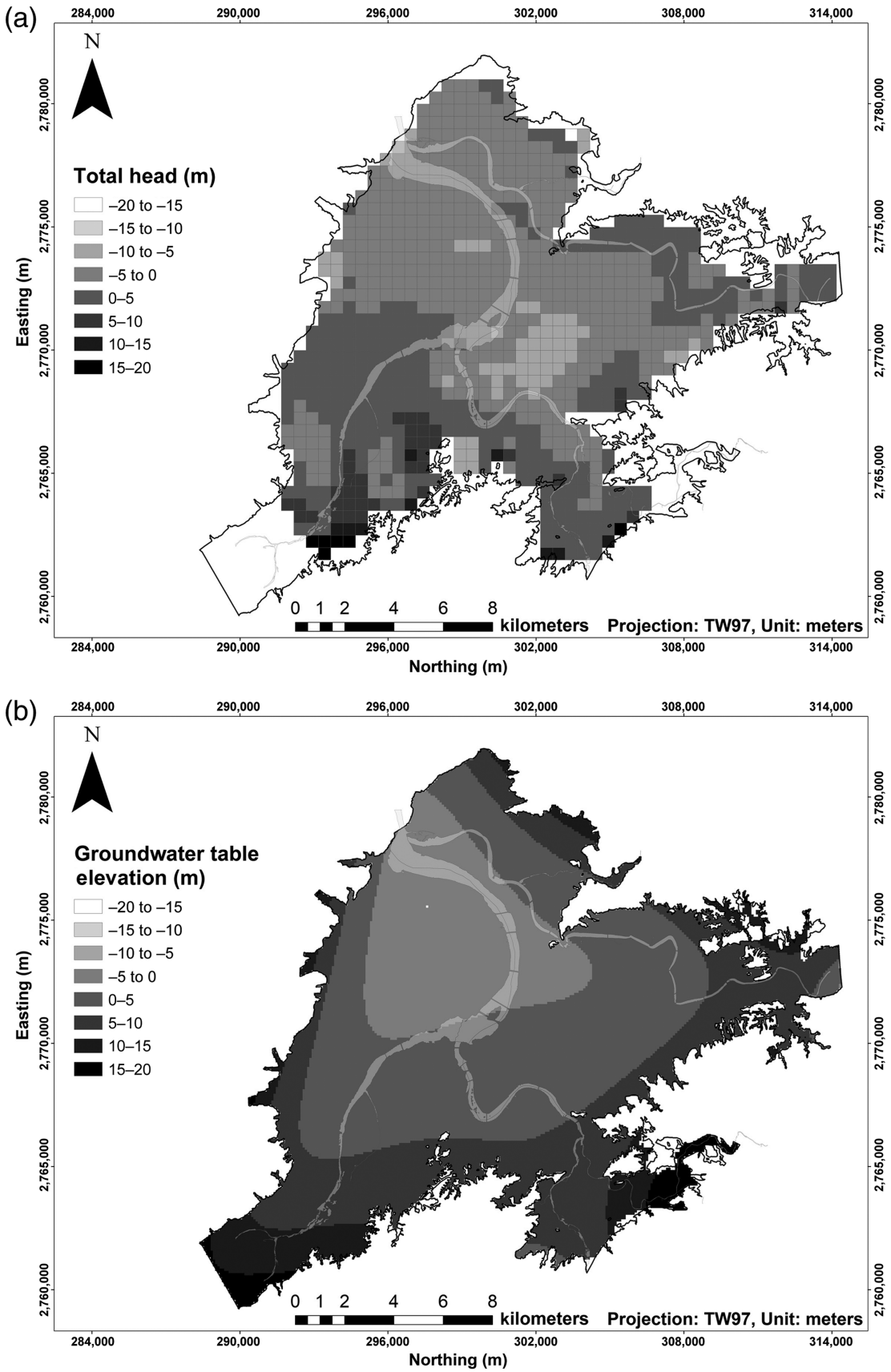

Figure 5. Groundwater elevation models (a) total head model from Groundwater Modeling System (GMS) modeling and (b) sixth-order trend surface analysis of groundwater table elevation in the Taipei basin.

Downloaded from http://pubs.geoscienceworld.org/ssa/bssa/article-pdf/115/5/2439/7295436/bssa-2025020.1.pdf by National Central Univ Library Serials Office user on 08 December 2025

increments of 45 cm, whereas V_S measurements were taken at 1 m intervals with depth increments of 0.5 m. In cases in which two V_S measurements corresponded to a single soil sample, the average V_S-value was used. However, if the difference between the two V_S-values exceeded 50 m/s, the data pair was excluded to avoid potential mismatches due to geological variability. The data pairing scheme is illustrated in Figure S1.

In addition, a two-step screening process was applied to ensure data reliability:

1. Quality screening: Only high-quality V_S measurements were retained, defined earlier as those with clear first arrivals and strong cross-correlation between opposite-direction traces, based on visual inspection and cross-correlation analysis.
2. Depth limitation: Samples deeper than 40 m were excluded to remove non-Holocene alluvial deposits, which do not significantly influence V_{S30}.

The impact of this screening process on the accuracy of the V_S estimation functions was assessed using rmse and R^2-values, as discussed in the results section. The final dataset initially comprised 173 soil–V_S data pairs, categorized into gravel (17), sand (51), silt (34), and clay (88) samples. However, to address the limited number of gravel samples, additional assumptions were made to increase the gravel soil–V_S data pairs to 171. This process involved incorporating previously excluded suboptimal V_S measurements and assuming a consistent unit weight for gravel layers in which soil test results were missing or unavailable. Further details on the gravel sample data preprocessing are provided in the supplemental material. The final soil–V_S data pairs were used in the regression analysis to develop separate void ratio- and effective stress-based V_S estimation functions for gravel, sand, silt, and clay.

V_{S30} calculation

Measured V_{S30} from EGDT data. For the EGDT database, V_{S30} was calculated directly from measured V_S-values, which were available at 0.5 m intervals. Of the 41 strong-motion stations within the Taipei basin, 40 were utilized, with TAP001 excluded due to missing measurement data. The top 30 m of measured V_S from the strong-motion stations were used to calculate V_{S30} using the following equation:

$$V_{S30} = \frac{30}{\sum_i^n \frac{d_i}{V_{Si}}}, \tag{4}$$

in which n is total number of layers, d_i is the thickness of the ith layer, and V_{Si} is the shear-wave velocity of the ith layer. V_{S30} can be categorized into site classes in building codes, such as in the U.S. National Earthquake Hazards Reduction Program (NEHRP) developed by the Federal Emergency Management Agency. In this study, the 1994 NEHRP standards (BSSC, 1995), as modified in Lee and Tsai (2008), were used instead of newer versions because they provide a finer scale of V_{S30} ranges, making it easier to observe changes in V_{S30} in the Taipei basin (Table 1).

TABLE 1
V_{S30} Site Classification Criteria (BSSC, 1995), as Modified by Lee and Tsai (2008)

Site Class	Range of V_{S30} (m/s)	Description
A	$V_{S30} > 1500$	Hard rock
B	$760 < V_{S30} \leq 1500$	Rock
C3	$620 < V_{S30} \leq 760$	Very dense soil and soft rock
C2	$490 < V_{S30} \leq 620$	
C1	$360 < V_{S30} \leq 490$	
D3	$300 < V_{S30} \leq 360$	Stiff soils
D2	$240 < V_{S30} \leq 300$	
D1	$180 < V_{S30} \leq 240$	
E	$V_{S30} < 180$	Soft soils

Estimated V_{S30} from CGS data. For the CGS boreholes, V_{S30} was estimated using the void ratio and effective stress-based V_S estimation functions developed in this study. Separate V_S estimation functions were applied to sand, silt, clay, and gravel layers, following a modified form of the Robertson *et al.* (1995) equation:

$$V_s = (m_1 - m_2 e)\left(\frac{\sigma_v'}{P_a}\right)^{n_a}, \tag{5}$$

in which m_1, m_2, and n_a are regression coefficients specific to each soil type, e is the void ratio, σ_v' is the effective vertical stress, and P_a is atmospheric pressure, set to a constant value of 100 kPa (Robertson *et al.*, 1995). Using these estimation functions, V_S-values were calculated at 1 m intervals from the surface to 30 m based on soil sample classification test results. For boreholes ≥30 m, V_{S30} was calculated using equation (4). However, for shallow boreholes (<30 m), the V_S profile was extrapolated to 30 m to calculate V_{S30}, as discussed in the following section. For boreholes where rock was present within the top 30 m, an average V_S of 600 m/s was assigned to the rock layer. This value was computed from the mean slowness (Kuo and Abrahamson, 2023) of rock columns based on direct V_S measurements from weathered and fresh Neogene rocks in the EGDT database. The V_S measurements used to calculate this average were all within the Taipei basin and corresponded to depths ranging from 3 to 38 m, with an average depth of ~20 m. In addition, due to the large amount of borehole data and challenges in identifying clear soil–rock boundaries, an interpolated basement rock elevation model for the Taipei basin was used to determine the boundary between soil and rock for each borehole (Lin, 2023) (Fig. 6).

Extrapolation of shallow V_S profiles. This study compares three V_S profile extrapolation methods for estimating V_{S30} at CGS boreholes shallower than 30 m: the bottom

Downloaded from http://pubs.geoscienceworld.org/ssa/bssa/article-pdf/115/5/2439/7295436/bssa-2025020.1.pdf by National Central Univ Library Serials Office user on 08 December 2025

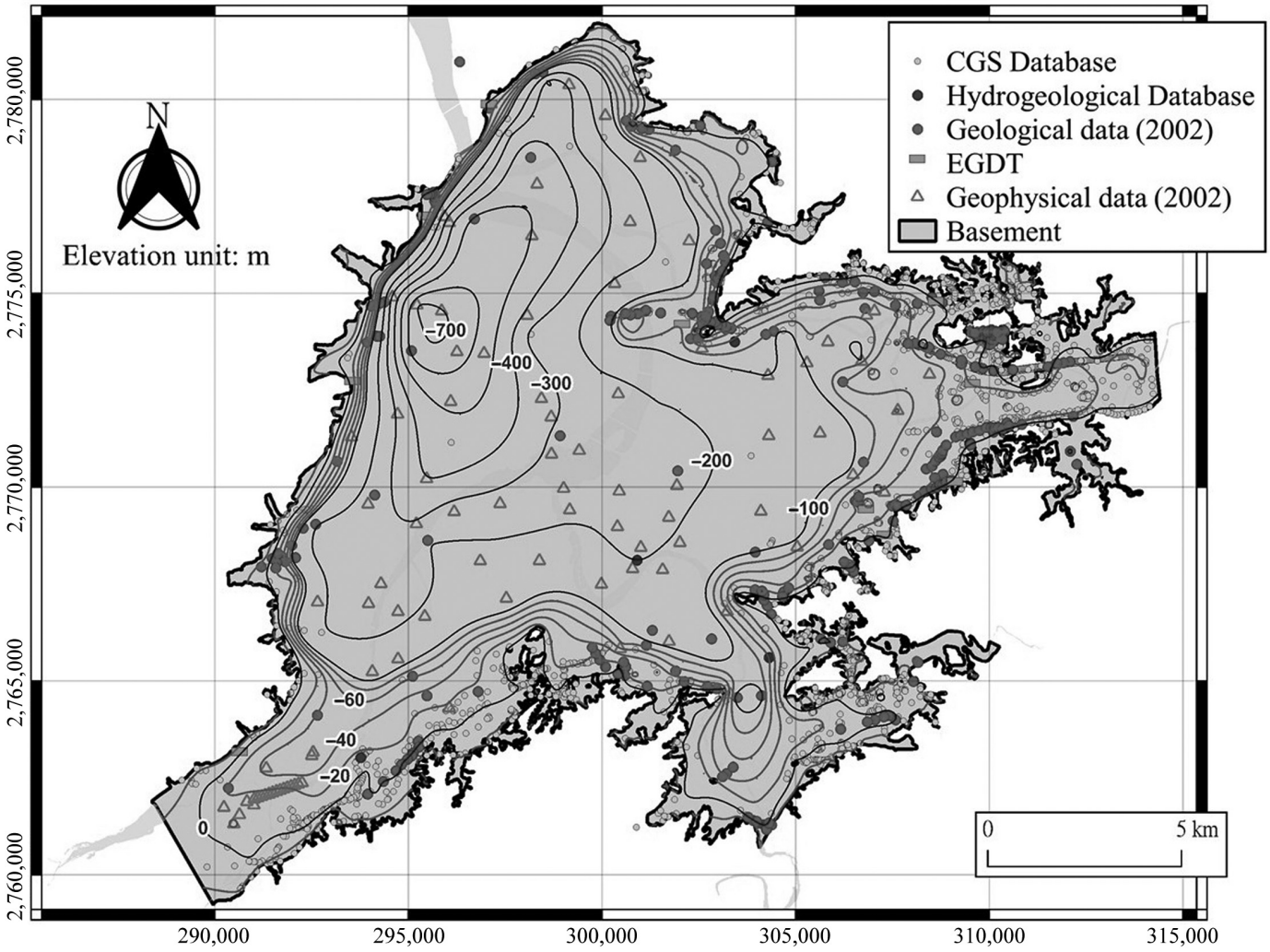

Figure 6. Contour map illustrating the elevation of the basement rock in the Taipei basin, based on the work by Lin (2023) using data from the Engineering Geological Exploration Database from the Central Geological Survey (CGS) (2002); EGDT (Kuo *et al.*, 2012); geological and geophysical data from Lee *et al.* (2002); Hydrogeological Database from the Taiwan Ministry of Economic Affairs (see Data and Resources). The red contour lines are at 20 m intervals, whereas the black lines are at 100 m intervals.

constant velocity (BCV) model, the CIP model, and the Boore *et al.* (2011) model.

The BCV model (Boore, 2004; Kuo *et al.*, 2011, 2012; Xie *et al.*, 2016) assumes that shear-wave velocity remains constant below the borehole depth to 30 m. The V_{S30} is calculated as

$$V_{S30} = \frac{30}{\Delta t_z + \frac{30 - z_p}{V_{S(z_p)}}}, \tag{6}$$

in which z_p is the depth of the V_S profile and Δt_z is the shear-wave travel time from z_p to the surface.

The CIP model (Dai *et al.*, 2013; Xie *et al.*, 2016) establishes a statistical relationship between instantaneous shear-wave velocity at a specific depth ($V_{S(Z_p)}$) and the average velocity from that depth to 30 m ($V_{S[Zp,30]}$), given by

$$\log V_{S[Zp,30]} = c_0 + c_1 \log V_{S(Z_p)}, \tag{7}$$

in which c_0 and c_1 are regression coefficients. V_{S30} is then calculated as

$$V_{S30} = \frac{30}{\Delta t_z + \frac{30 - z_p}{V_{S[z_p,30]}}}. \tag{8}$$

The Boore *et al.* (2011) model predicts V_{S30} using the relationship between average velocity at depths less than 30 m (V_{Sz}) and V_{S30}, incorporating a dummy variable (δ_E) to account for systematic differences in class E sites ($V_{S30} < 180$ m/s):

$$\log V_{S30} = c_{oE}\delta_E + c_0 + c_1 \log V_{Sz} + c_2 (\log V_{Sz})^2, \tag{9}$$

in which c_0, c_1, and c_2 are regression coefficients and c_{oE} is the coefficient for the dummy variable δ_E, which equals 1 for class E sites and 0 for non-class E sites.

To assess the accuracy of these methods, 29 V_S profiles from EGDT strong-motion stations within the Taipei basin were used, whereas stations with insufficient depth (<30 m), incomplete V_S profiles, or rock present within the top 30 m were

Downloaded from http://pubs.geoscienceworld.org/ssa/bssa/article-pdf/115/5/2439/7295436/bssa-2025020.1.pdf by National Central Univ Library Serials Office user on 08 December 2025

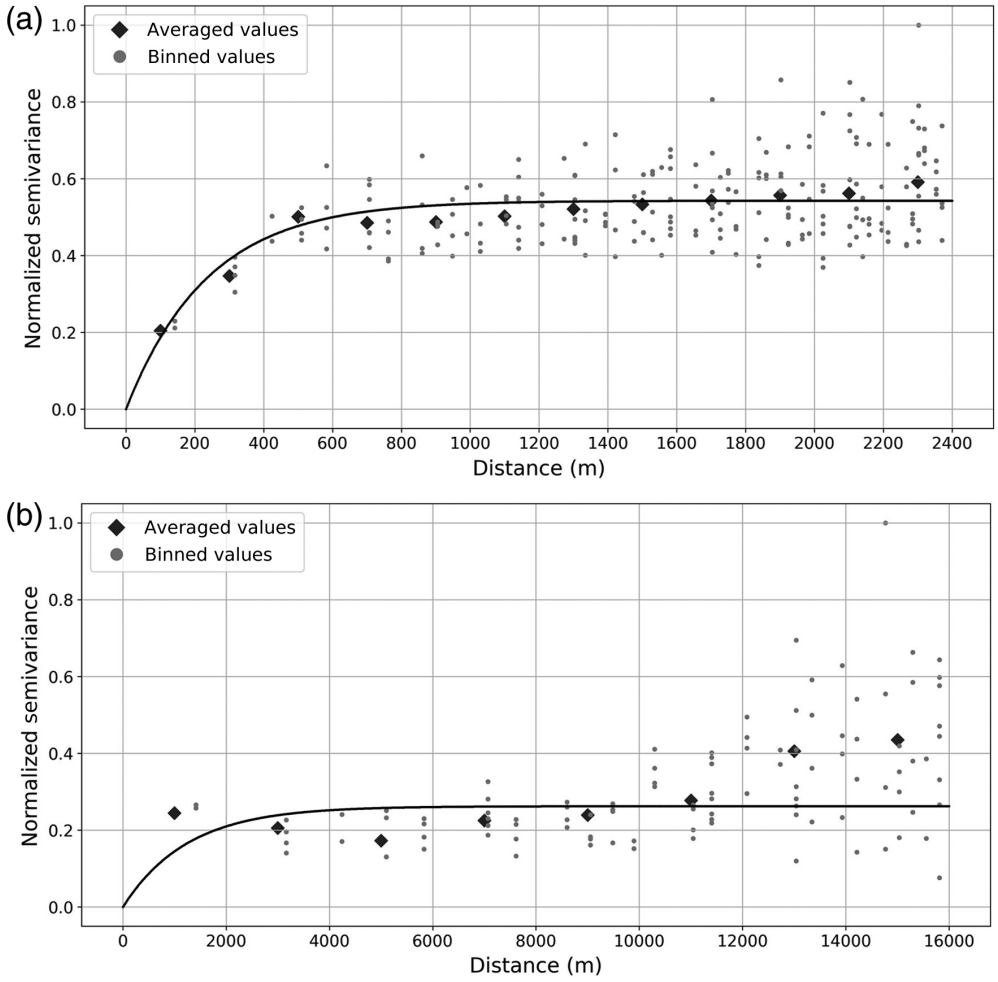

Figure 7. Semivariograms for (a) estimated V_{S30} from CGS data (auxiliary variable) and (b) measured V_{S30} from EGDT data (primary variable).

excluded to ensure reliable comparisons. For each strong-motion station used, the V_S profile was artificially truncated at depths ranging from 10 to 29 m, in 1 m increments (i.e., extrapolations were performed from 10 to 30 m, 11 to 30 m, …, up to 29 to 30 m). The BCV, CIP, and Boore *et al.* (2011) methods were then applied directly to the truncated profiles to estimate V_{S30}. The accuracy of each method was evaluated by comparing the estimated V_{S30}-values with the true measured V_{S30} at the corresponding strong-motion stations.

V_{S30} mapping: Kriging with varying local means

This study employed Kriging with varying local means to interpolate V_{S30}-values in the Taipei basin. Previous studies have successfully applied this method for V_{S30} interpolation in various regions of Taiwan (Lee and Tsai, 2008). This technique combines auxiliary data, in this case estimated V_{S30}-values from V_S estimation functions, with residual corrections derived from measured V_{S30} at strong-motion stations. Although simpler and more computationally efficient methods, such as ordinary Kriging, are available, they often fail to capture local variations, which are critical for accurately identifying areas at risk of site effects.

The spatial interpolation process using Kriging with varying local means consisted of three main steps:

Step 1: Kriging interpolation of auxiliary variables: The estimated V_{S30}-values, derived from the engineering boreholes (CGS data) using the void ratio- and effective stress-based V_S estimation functions, were interpolated using Kriging to generate a grid of auxiliary variable data by estimating values at unsampled locations. Typically, Kriging with varying local means requires a regression analysis to establish the correlation between the primary and auxiliary variables. However, this step was unnecessary in our study because both variables represented V_{S30}-values. For this step, the semi-variogram used an exponential model with a lag size of 200 m, based on data fitting and the average distance between CGS boreholes (Fig. 7a).

Step 2: Residual calculation and interpolation: Residual values were calculated by subtracting the measured V_{S30}-values (EGDT data) at strong-motion station locations (primary variable) from the auxiliary variable grid values generated in step 1. Kriging was then applied to interpolate the residual values and produce a residual map. Similar to step 1, this step used an exponential semi-variogram model; however, the lag size was set to 2500 m, corresponding to the average distance between the strong-motion stations (Fig. 7b).

Step 3: Development of V_{S30} map: The final V_{S30} map was developed by adding the residual map (step 2) to the auxiliary variable grid (step 1), resulting in the spatial distribution of V_{S30} generated through Kriging with varying local means.

RESULTS

Shear-wave velocity estimation functions

A single multivariate regression was performed in which shear-wave velocity was modeled simultaneously as a function of void ratio and vertical effective stress (equation 5), producing

Downloaded from http://pubs.geoscienceworld.org/ssa/bssa/article-pdf/115/5/2439/7295436/bssa-2025020.1.pdf by National Central Univ Library Serials Office user on 08 December 2025

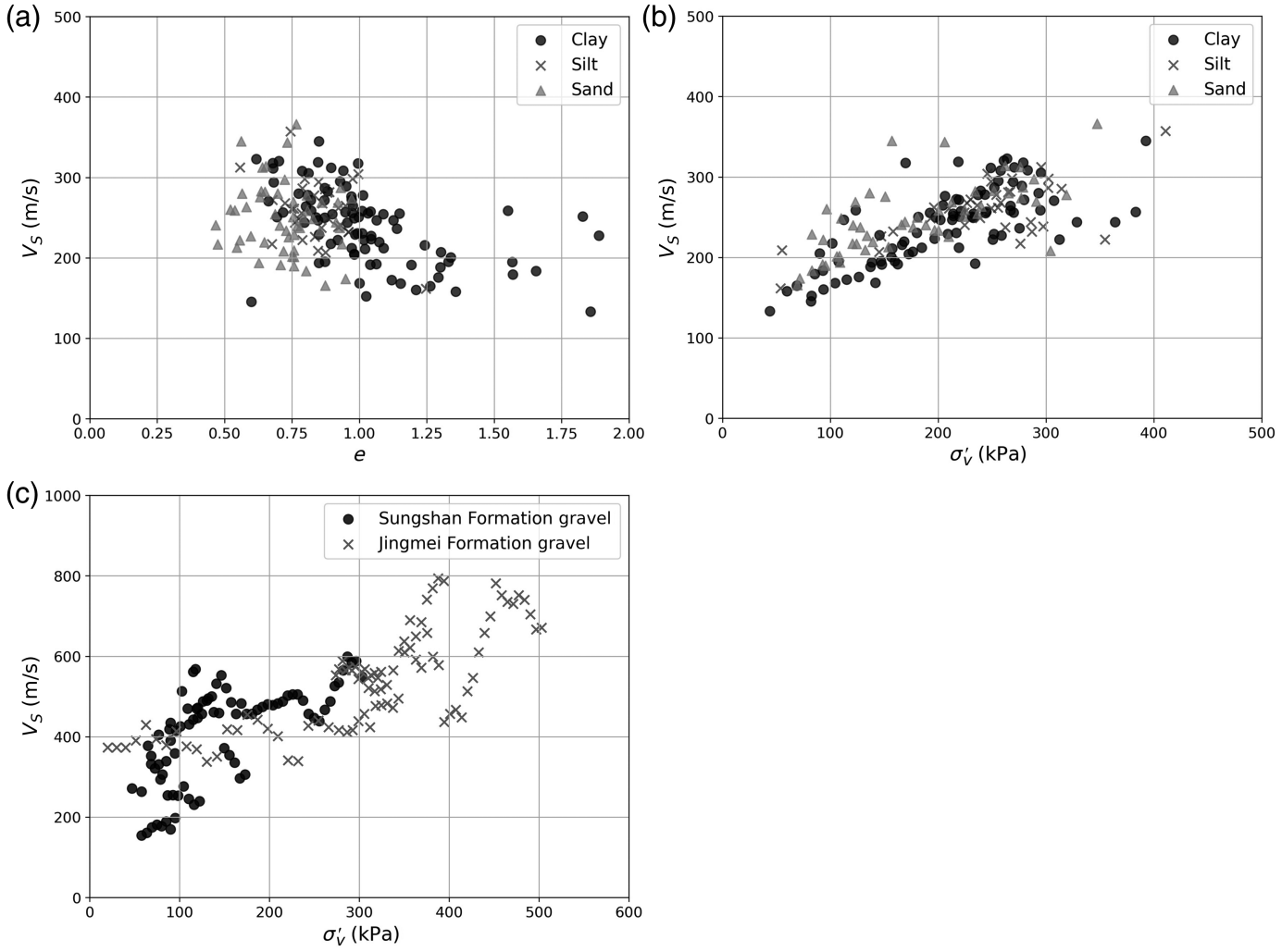

Figure 8. Correlation between soil parameters and shear-wave velocity. (a) Correlation between e and V_S for sand, clay, and silt; (b) correlation between σ'_v and V_S for sand, clay, and silt; and (c) correlation between σ'_v and V_S for gravel of the Sungshan and Jingmei Formations.

lithology-specific V_S estimation functions for gravel, sand, silt, and clay. These functions demonstrated strong correlations between V_S and both void ratio and vertical effective stress, as shown in Figure 8 and summarized in Table 2. For the sand, silt, and clay soil–V_S data pairs, the two-step screening process of retaining only high-quality V_S measurements and excluding samples deeper than 40 m improved the accuracy of the V_S estimation functions significantly. This was reflected in the rmse decreasing from 50.82 to 30.80 m/s for sand, from 44.83 to 26.52 m/s for silt, and from 66.88 to 29.88 m/s for clay, highlighting the effectiveness of the filtering criteria in reducing estimation errors. The relatively higher rmse value for gravel (86.70 m/s) is likely due to the inclusion of suboptimal V_S measurements (used to increase the limited gravel dataset), combined with its naturally wide variation in particle size, shape, and packing, which together resulted in greater variability in estimated V_S. In addition, the void ratio was excluded from the gravel V_S estimation function due to the lack of a statistically significant correlation between void ratio and V_S for gravel samples. Unlike finer-grained soils such as sand, silt, and clay, gravel tends to have a loose structural arrangement, leading to weak or inconsistent relationships between void ratio and shear-wave velocity. Instead, V_S for gravel was modeled based solely on effective vertical stress. From the effective-stress exponents, gravel (0.38) exhibits the greatest sensitivity to variations in confining stress, followed by clay (0.33), sand (0.28), and silt (0.23). A higher exponent indicates that a given increase in effective stress leads to a

TABLE 2
Shear-Wave Velocity Estimation Functions for Gravel, Sand, Silt, and Clay

Soil Type	Estimation Function	Rmse (m/s)	R^2
Gravel	$V_S = (360.6)(\frac{\sigma'_v}{100})^{0.38}$	86.70	0.60
Sand	$V_S = (240.5 - 35.9e)(\frac{\sigma'_v}{100})^{0.28}$	30.80	0.44
Silt	$V_S = (230.2 - 21.1e)(\frac{\sigma'_v}{100})^{0.23}$	26.52	0.46
Clay	$V_S = (213.1 - 21.3e)(\frac{\sigma'_v}{100})^{0.33}$	29.86	0.60

Rmse, root mean square error.

Downloaded from http://pubs.geoscienceworld.org/ssa/bssa/article-pdf/115/5/2439/7295436/bssa-2025020.1.pdf by National Central Univ Library Serials Office user on 08 December 2025

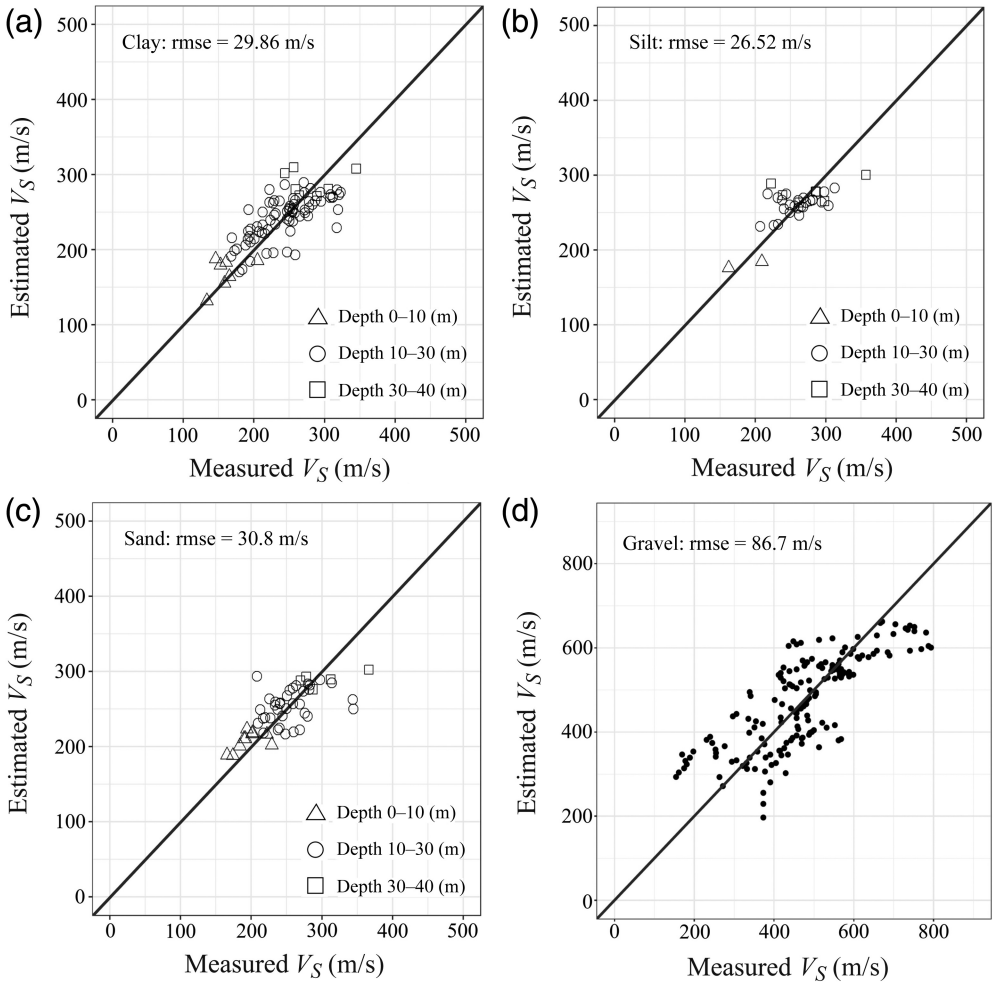

Figure 9. Comparison of estimated and measured V_S-values for (a) clay, (b) silt, (c) sand, and (d) gravel.

proportionally larger rise in stiffness, and thus in shear-wave velocity. In contrast, the negative void-ratio coefficients for sand (−35.9), silt (−21.1), and clay (−21.3) indicate that higher void ratios, reflecting looser packing, correspond to lower shear-wave velocities. These findings underscore that coarser gravelly soils depend more strongly on effective stress, whereas finer-grained soils also require explicit consideration of void ratio in capturing their shear-wave velocity behavior.

To validate the estimation functions proposed in this study, V_S-values estimated from soil parameters at EGDT strong-motion stations were compared with directly measured V_S-values at the same locations, as shown in Figure 9. The results demonstrate strong agreement between estimated and measured V_S across all soil types. Although gravel exhibited greater variation due to limited high-quality V_S measurements, and factors such as compaction and sorting, the proposed function still showed a reasonable correlation with measured values.

To further evaluate the accuracy of the proposed V_S estimation functions, we compare our results with previous studies by Kuo *et al.* (2011), Lee and Tsai (2008), and Robertson *et al.* (1995) (Table 3), using the EGDT soil sample data and corresponding measured V_S-values. Robertson *et al.* (1995) developed estimation functions based on the correlation between effective stress, void ratio, and shear-wave velocity, whereas Kuo *et al.* (2011) and Lee and Tsai (2008) utilized correlations between SPT-N values and shear-wave velocity. Notably, Robertson's study focused solely on sand, which likely increases error when applied to other soil types. In contrast, Kuo *et al.* (2011) and Lee and Tsai (2008) proposed estimation functions for sand as well as combined functions for silt and clay. Overall, our proposed estimation functions show improved rmse for sand, silt, and clay (Figs. 10 and 11). Gravel was excluded from the comparison because it was not considered in previous studies. It is also important to note that regional factors also influence the accuracy of estimation functions. Kuo *et al.* (2011) and Lee and Tsai (2008) used Taipei basin data, whereas Robertson's study was based on Ottawa Sand. Differences in sedimentary composition, depositional environments, and tectonic

TABLE 3
Shear-Wave Velocity Estimation Functions from Previous Studies

	Shear-Wave Velocity Estimation Functions		
Author	**Clay**	**Silt**	**Sand**
This study	$V_S = (213.1 - 21.3e)(\frac{\sigma'_v}{100})^{0.33}$	$V_S = (230.2 - 21.1e)(\frac{\sigma'_v}{100})^{0.23}$	$V_S = (240.5 - 35.9e)(\frac{\sigma'_v}{100})^{0.28}$
Robertson *et al.* (1995)	–		$V_S = (381 - 259e)(\frac{\sigma'_v}{100})^{0.26}$
Lee and Tsai (2008)	$V_S = 163.149N^{0.192}$		$V_S = 98.067N^{0.305}$
Kuo *et al.* (2011)	$V_S = 114.55N^{0.168}D^{0.143}$		$V_S = 93.11N^{0.242}D^{0.136}$

Downloaded from http://pubs.geoscienceworld.org/ssa/bssa/article-pdf/115/5/2439/7295436/bssa-2025020.1.pdf by National Central Univ Library Serials Office user on 08 December 2025

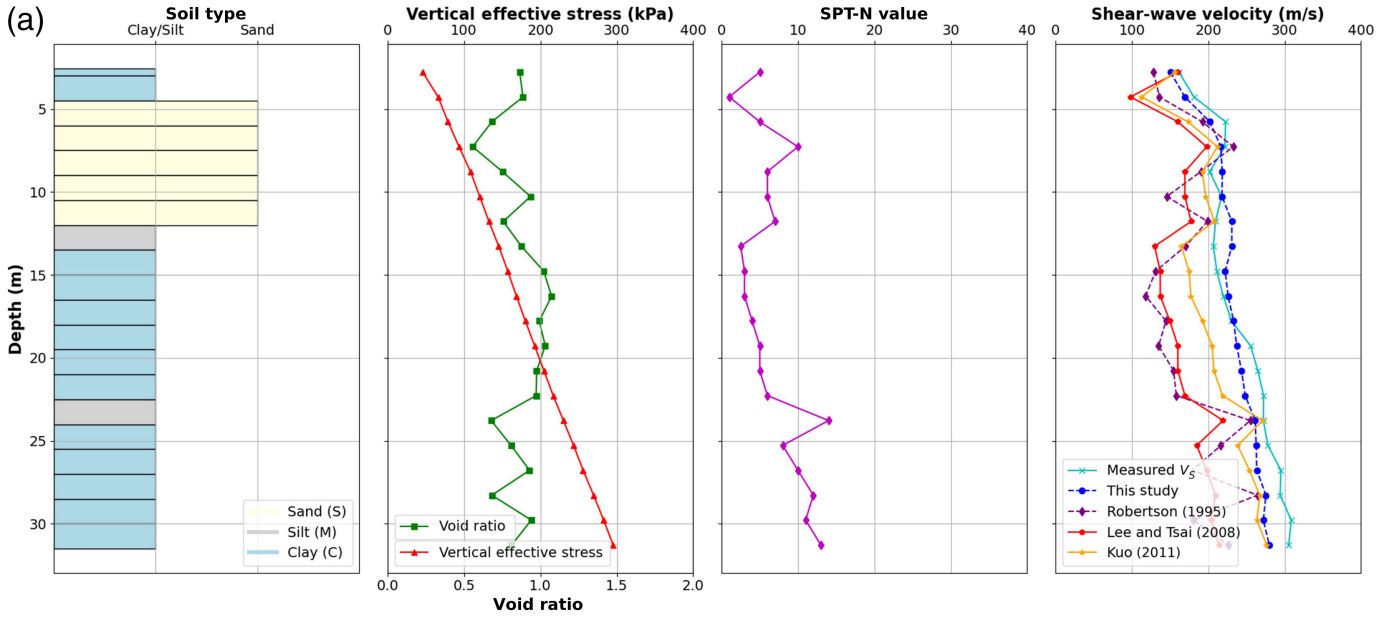

Estimation function	This study	Robertson *et al.* (1995)	Lee and Tsai (2008)	Kuo *et al.* (2011)
Rmse (m/s)	19.0	76.1	77.0	38.5

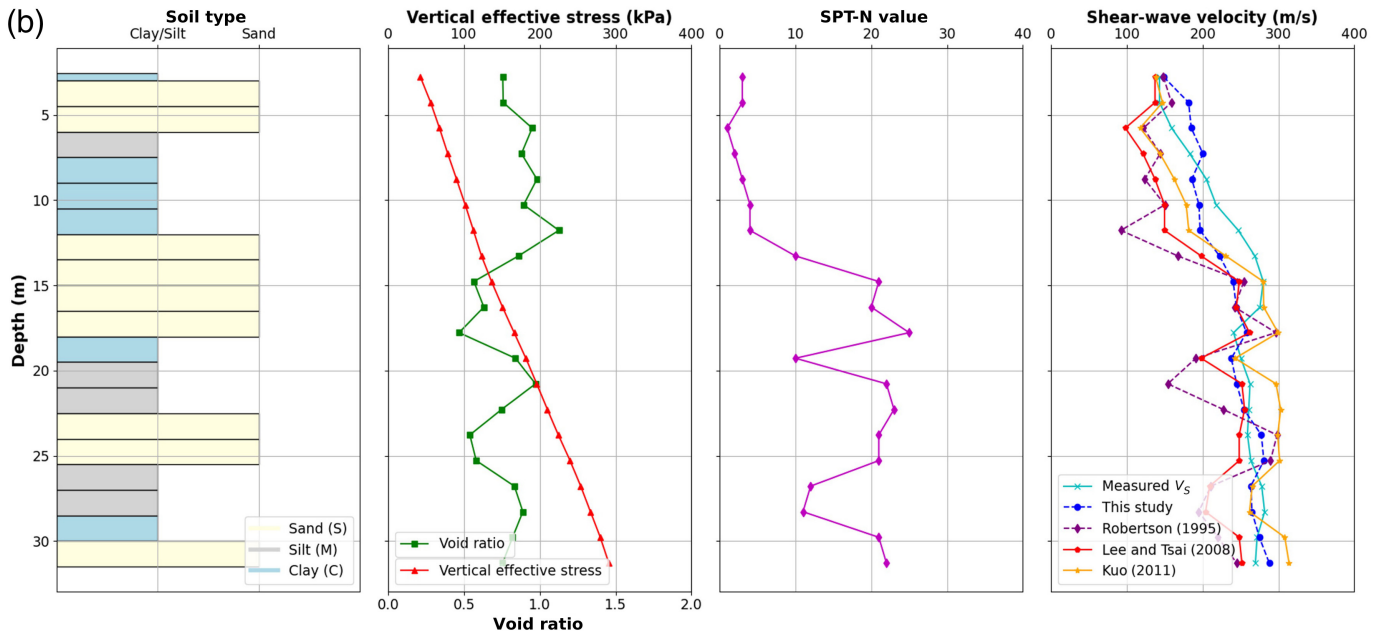

Estimation function	This study	Robertson *et al.* (1995)	Lee and Tsai (2008)	Kuo *et al.* (2011)
Rmse (m/s)	25.4	66.1	49.3	35.9

history, such as those observed in the Fraser River Delta in Canada or the Kanto Plain in Japan, affect soil properties and consequently V_{S30}-values. Therefore, estimation functions should be calibrated using local data and updated as new measurements become available to improve accuracy. Another important consideration is the inherent uncertainty associated with both void ratio and groundwater level (used to determine effective stress),

Figure 10. Comparison of shear-wave velocity estimation compared to previous studies, using (a) strong-motion station TAP020 and (b) strong-motion station TAP037. The color version of this figure is available only in the electronic edition.

Downloaded from http://pubs.geoscienceworld.org/ssa/bssa/article-pdf/115/5/2439/7295436/bssa-2025020.1.pdf by National Central Univ Library Serials Office user on 08 December 2025

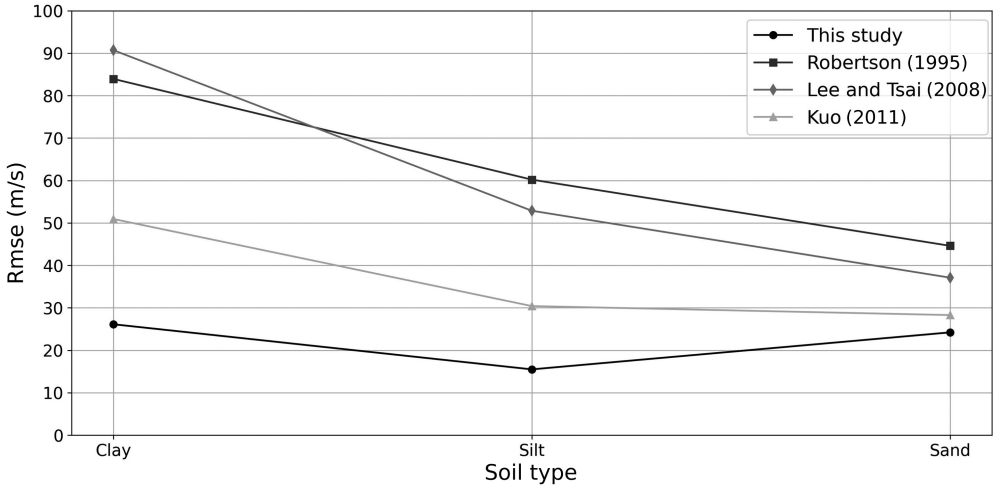

Figure 11. Root mean square error (rmse) for different soil types compared to previous studies.

due to variability in sampling methods, local soil heterogeneity, and temporal fluctuations. These uncertainties may introduce variability in the final V_{S30} predictions, and their potential impacts are examined in the Discussion section.

V_{S30} calculation

Measured V_{S30} from EGDT data. For the EGDT dataset, V_{S30}-values were calculated directly from measured V_S profiles. The spatial distribution of V_{S30} at EGDT strong-motion stations in the Taipei basin is shown in Figure 12.

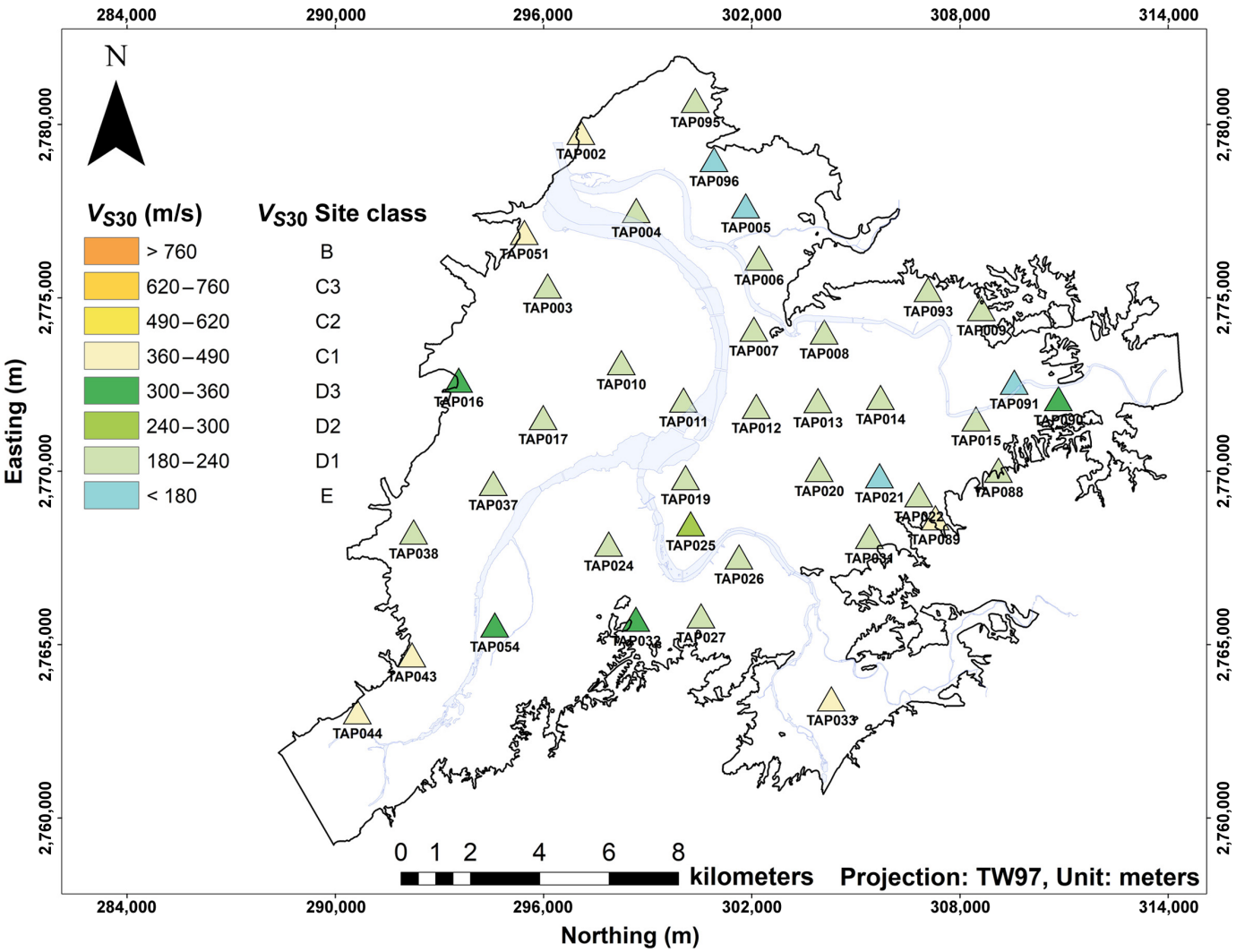

Figure 12. V_{S30} at each borehole from the strong-motion stations (EGDT), estimated by equation (9). These values will serve as the primary variable for the interpolation of the V_{S30} map. The color version of this figure is available only in the electronic edition.

Downloaded from http://pubs.geoscienceworld.org/ssa/bssa/article-pdf/115/5/2439/7295436/bssa-2025020.1.pdf by National Central Univ Library Serials Office user on 08 December 2025

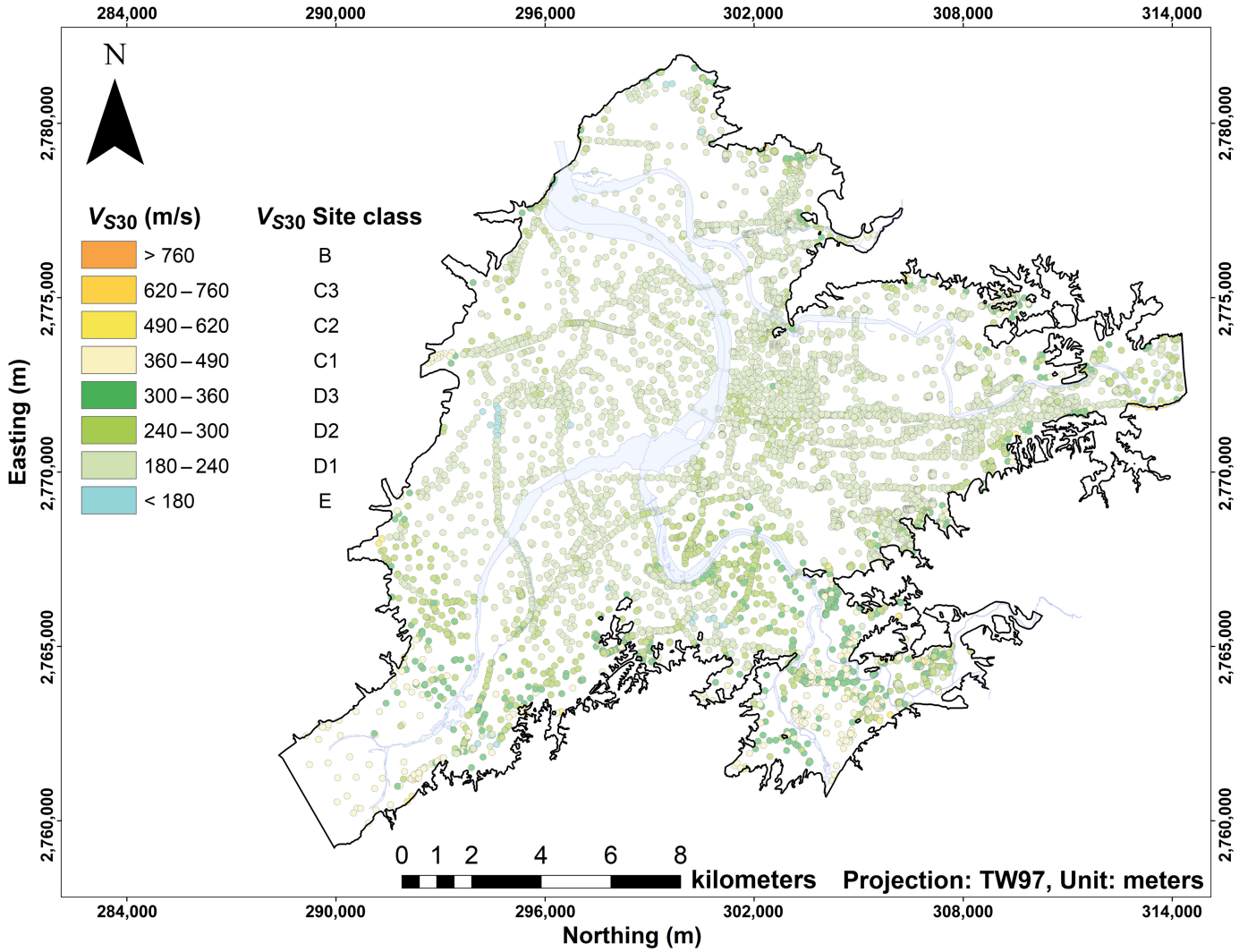

Figure 13. V_{S30} of 6766 boreholes from CGS boreholes, including shallow boreholes for which the conditional independent property (CIP) model was used to extrapolate shear-wave velocity to 30 m. These values will serve as the auxiliary variable for the interpolation of the V_{S30} map. The color version of this figure is available only in the electronic edition.

Using the NEHRP site classification criteria (BSSC, 1995), as modified by Lee and Tsai (2008) and summarized in Table 1, most V_{S30}-values fall within the range of 180–360 m/s. However, four boreholes (TAP005, TAP021, TAP091, and TAP096) located in the northern and eastern parts of the basin exhibited V_{S30}-values below 180 m/s. These low V_{S30}-values can be attributed to the subsurface conditions at these locations, which are characterized by thick clay layers that extend through the full V_{S30} calculation depth and, in most cases, continue deeper. The clay at these sites also exhibited very low SPT-N values, typically around 5, with a maximum of 10, indicating very soft and weak soil. Such low stiffness and high compressibility are consistent with the low shear-wave velocities observed, and explain the resulting V_{S30}-values falling within NEHRP site class E. This classification indicates that these stations are subject to the highest potential for amplified ground shaking during earthquakes. Conversely, six boreholes (TAP002, TAP033, TAP043, TAP044, TAP051, and TAP089) near the basin margins displayed V_{S30}-values between 490 and 620 m/s. At TAP033 and TAP043, the elevated V_{S30}-values are due to thick gravel sequences, whereas the other high V_{S30}-value stations are due to the presence of shallow bedrock within the top 30 m of the ground.

Estimated V_{S30} from CGS. For the CGS borehole data, V_{S30}-values were estimated using the proposed void ratio- and effective stress-based V_S estimation functions. The results show that in the central basin, V_{S30}-values predominantly range from 180 to 360 m/s, reflecting the thick sequence of fine-grained Holocene deposits in this region (Fig. 13), and aligning with the measured V_{S30}-values from the EGDT dataset. This range also agrees with earlier seismic reflection results by Wang *et al.* (2004), who found that shear-wave velocities within the upper Sungshan Formation generally ranged from 170 to 340 m/s (Fig. S2), consistent with the V_S-values estimated in this study.

Downloaded from http://pubs.geoscienceworld.org/ssa/bssa/article-pdf/115/5/2439/7295436/bssa-2025020.1.pdf by National Central Univ Library Serials Office user on 08 December 2025

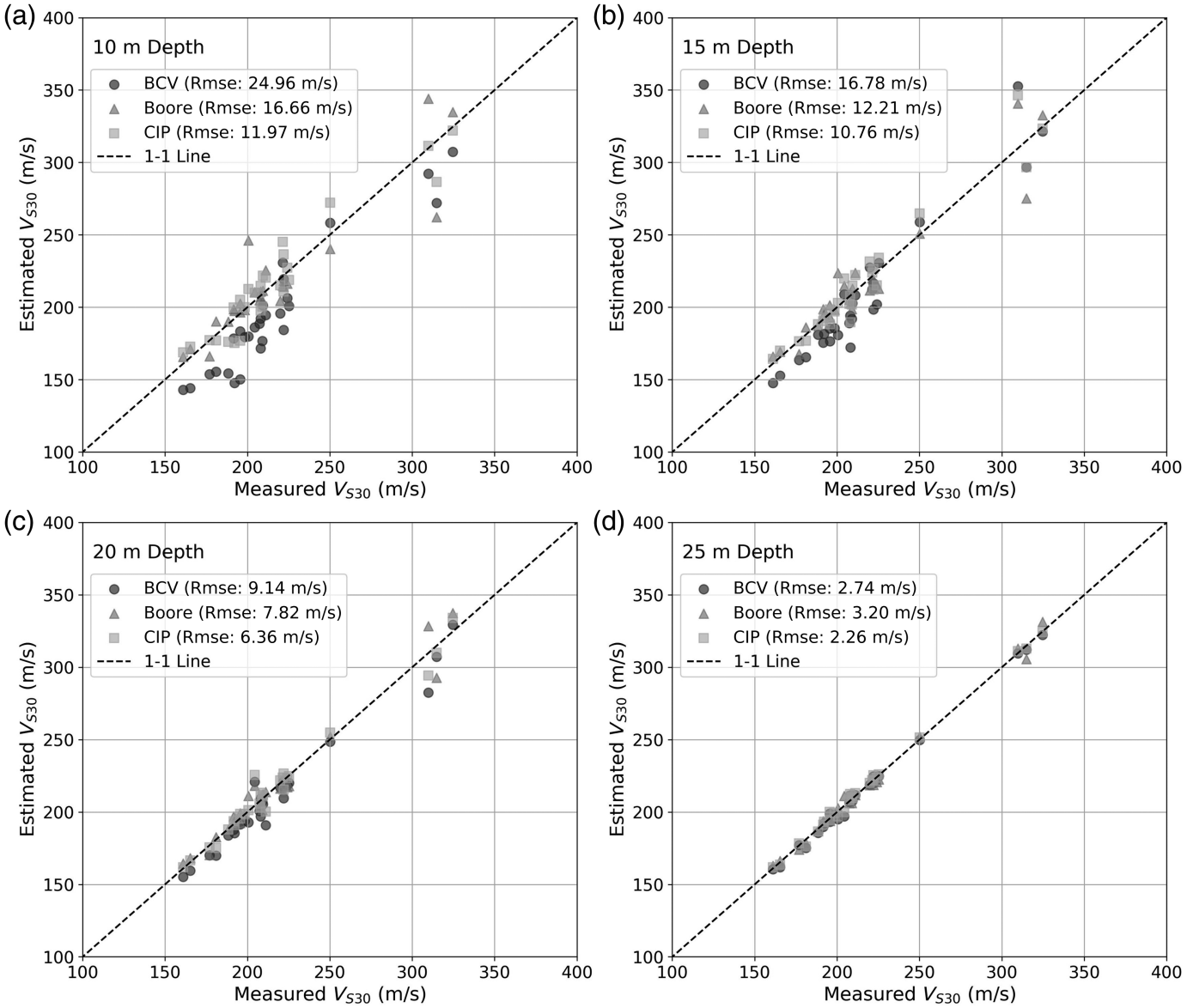

Figure 14. Comparison between the extrapolated V_{S30} results from the bottom constant velocity (BCV), CIP, and Boore *et al.* (2011) models from depths of (a) 10, (b) 15, (c) 20, and (d) 25 m, illustrating the V_{S30}-values obtained from the models and the measured V_{S30}-values.

Lower estimated V_{S30}-values (<180 m/s) are predominantly observed in the northern and eastern parts of the basin, corresponding to areas with thicker soft alluvial sediments. These lower values indicate the potential for significant site amplification effects. However, because V_{S30} does not directly account for deep sediment thickness, long-period site effects in the central basin may require additional geophysical characterization. In contrast, higher V_{S30}-values (490–620 m/s) are observed near the basin margins, due to shallow bedrock or coarse-grained deposits such as gravel layers.

Because V_{S30} is a depth-averaged parameter, improved accuracy in layer-specific V_S estimates translates directly into more reliable V_{S30}-values. Compared to previous SPT-based methods (Lee and Tsai, 2008; Kuo *et al.*, 2011), the V_S-values and consequently the V_{S30} estimates derived in this study from void ratio and effective stress show improved accuracy (Fig. 11). Furthermore, the proposed method allows for significantly greater V_{S30} data density within the Taipei basin by enabling the use of a broader range of engineering boreholes, including those that lack reliable SPT measurements.

Extrapolation of shallow V_S profiles. Of the 6766 CGS boreholes in the Taipei basin, 2850 have depths of less than 30 m, requiring the V_S profiles to be extrapolated to 30 m for deriving V_{S30}. Three extrapolation methods were evaluated; the BCV model, the CIP model, and the Boore *et al.* (2011) model. The CIP method yielded the best results, as shown in Figure 14, with estimated V_{S30}-values closely matching measured V_{S30}. In contrast, the BCV and Boore *et al.* (2011) methods occasionally underestimated V_{S30}. In many cases, V_S increases with depth as a

Downloaded from http://pubs.geoscienceworld.org/ssa/bssa/article-pdf/115/5/2439/7295436/bssa-2025020.1.pdf by National Central Univ Library Serials Office user on 08 December 2025

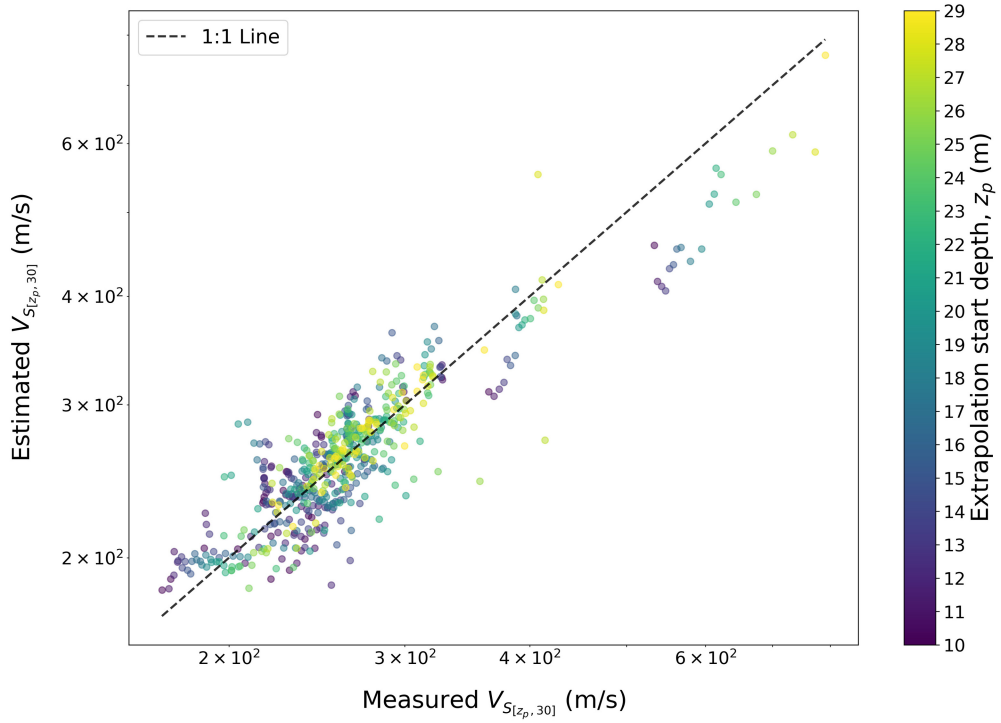

Figure 15. Correlation between estimated and measured $V_{S[z_p,30]}$-values at 28 strong-motion stations. The estimated values are extrapolated from different depths (z_p) to 30 m. The color version of this figure is available only in the electronic edition.

TABLE 4
Summary of the Linear Regression Results from the CIP Model

Depth	C_0	C_1	R^2	$\sigma_{residual}$ (LN scale)
10	0.74	0.71	0.81	0.097
11	0.91	0.64	0.70	0.122
12	0.84	0.67	0.68	0.126
13	0.91	0.64	0.67	0.128
14	0.74	0.71	0.74	0.113
15	0.76	0.70	0.76	0.108
16	0.70	0.73	0.77	0.106
17	0.63	0.76	0.82	0.092
18	0.53	0.80	0.79	0.099
19	0.45	0.83	0.77	0.104
20	0.44	0.83	0.79	0.100
21	0.49	0.81	0.80	0.098
22	0.33	0.88	0.85	0.084
23	0.19	0.93	0.90	0.069
24	0.21	0.92	0.84	0.090
25	0.23	0.92	0.80	0.103
26	0.25	0.90	0.78	0.102
27	0.17	0.94	0.87	0.113
28	0.27	0.89	0.97	0.089
29	0.06	0.98	0.99	0.044

CIP, conditional independent property.

result of increasing effective stress and compaction. However, the BCV method assumes that the last measured V_S at the base of the borehole remains constant to 30 m. Therefore, if the final V_S measurement is taken from a soft or transitional layer (e.g., clay or loose sand), and stiffer layers below are not captured, the model fails to reflect the natural velocity gradient, leading to underestimation of the true V_{S30}. Similarly, the Boore *et al.* (2011) model is based on empirical relationships derived from geological settings that differ from those in the Taipei basin. In this region, the soil profile often includes thick, soft alluvial clays, or loose silts that are not well represented in Boore's dataset. As a result, the model may underrepresent the increase in shear-wave velocity with depth, particularly when shallow layers exhibit very low velocities, leading to underestimation of V_{S30}. Consequently, the CIP model was selected for the extrapolation of shallow V_S profiles in this study because it provided the most statistically accurate representation of the increase in shear-wave velocity with depth.

Using the EGDT strong-motion station data, Figure 15 shows the correlation between measured and CIP-estimated average shear-wave velocities from various depths (z_p) to 30 m ($V_{S[Zp,30]}$). The results of this show an almost 1:1 correlation, which provides further evidence of the accuracy of extrapolating V_S using the CIP model. Notably, a cluster of points in the upper right portion of Figure 15, in which estimated $V_{S[Zp,30]}$-values are consistently lower than measured values, corresponds to strong-motion station TAP033. This station is characterized by a thick gravel deposit extending from ~3 to 30 m. However, this layer appears relatively heterogeneous, with the SPT-N values at or above 50 from 3 to 12 m, then decreasing sharply to about 20 between 12 and 22 m before increasing again. This unexpected drop in N-values within a gravelly deposit may reflect variations in compaction, grading, or the presence of finer material within the matrix, which can reduce stiffness and consequently lower the measured V_S at those depths. These lower measured V_S-values between 12 and 22 m could explain why the CIP model underestimates the extrapolated V_S at this site. This case highlights the complexity of interpreting V_S in heterogeneous coarse-grained materials.

Downloaded from http://pubs.geoscienceworld.org/ssa/bssa/article-pdf/115/5/2439/7295436/bssa-2025020.1.pdf by National Central Univ Library Serials Office user on 08 December 2025

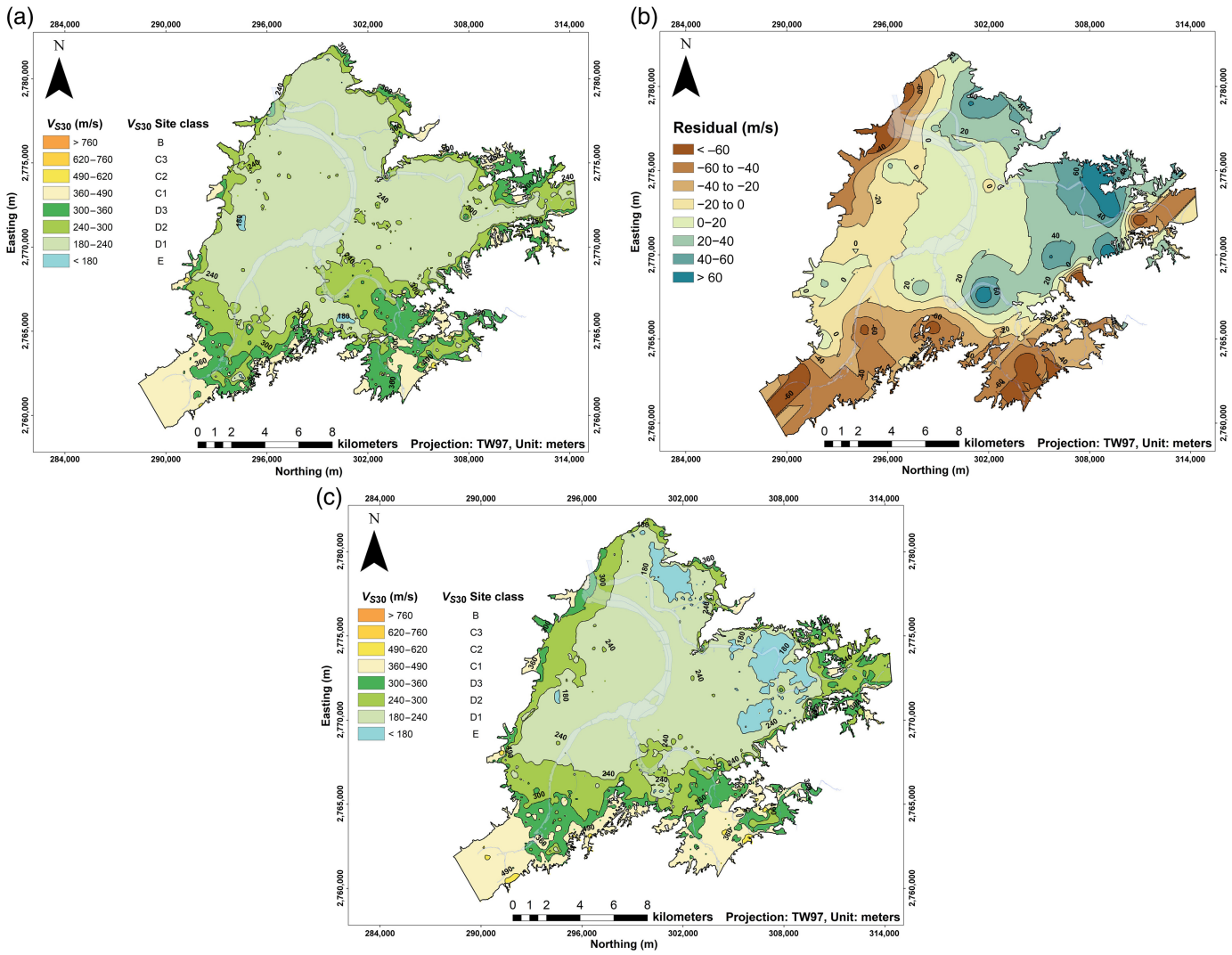

Figure 16. Results of the spatial interpolation process, consisting of the three steps. (a) Step 1: Kriging interpolation of auxiliary variables using V_{S30}-values from CGS data. (b) Step 2: residual map obtained by applying Kriging to each residual in the strong-motion stations. (c) Step 3: The final result of the V_{S30} map obtained using Kriging with varying local means. The color version of this figure is available only in the electronic edition.

To quantify the precision of the CIP model, the R^2-values and standard deviation of residuals (σ_{residual}) were calculated at each strong-motion station for depths between 10 and 29 m (Table 4). The formula to compute the σ_{residual} is as follows:

$$\sigma_{\text{residual}} = \sqrt{\frac{1}{N}\sum_{i=1}^{N}(\text{residual})_i^2}$$

$$\text{Residual} = (\log V_{S[Z_p,30]\text{Est}} - \log V_{S[Z_p,30]\text{Obs}}), \qquad (10)$$

in which N is the number of samples, $V_{S[Z_p,30]\text{Est}}$ is the estimated $V_{S[Z_p,30]}$, and $V_{S[Z_p,30]\text{Obs}}$ is the observed value.

The σ_{residual}-values, presented in Table 4, ranged from 0.0442 to 0.1258, indicating high precision and consistency in the CIP model's predictions. However, while σ_{residual} exhibited a moderate negative correlation with depth, the decrease was not consistent. This variability can be attributed to subsurface heterogeneity, particularly in the transition zone between sand and clay typically observed between 11 and 13 m in the Taipei basin, in which σ_{residual}-values tend to increase.

V_{S30} mapping: Kriging with varying local means

The Kriging with varying local means interpolation results revealed V_{S30}-values in the Taipei basin range from 150 to 600 m/s (Fig. 16). Identifying areas with low V_{S30}-values is crucial because these regions are more prone to site amplification effects due to materials with lower stiffness, which tend to resonate more with seismic waves, increasing their amplitude. This can lead to higher accelerations, longer shaking durations, and larger displacements compared to areas with higher shear-wave velocities. On the other hand, areas with higher V_{S30}-values, such as hard rock or more compacted soils, tend to experience less amplification and, as a result, generally exhibit lower levels of ground shaking during earthquakes. Two

Downloaded from http://pubs.geoscienceworld.org/ssa/bssa/article-pdf/115/5/2439/7295436/bssa-2025020.1.pdf by National Central Univ Library Serials Office user on 08 December 2025

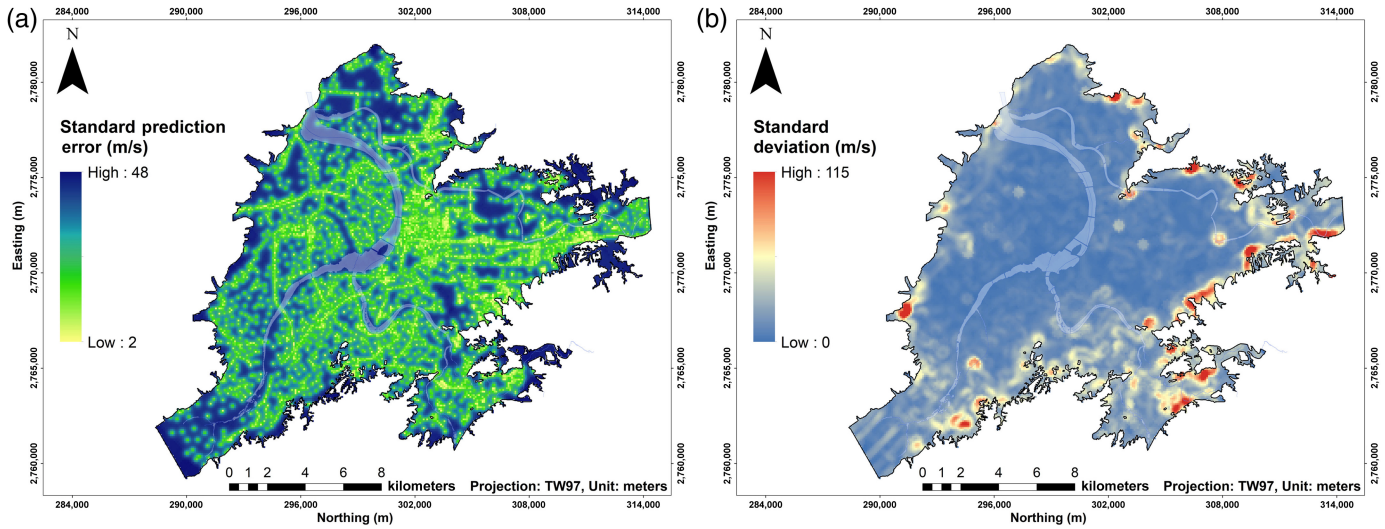

Figure 17. (a) Standard prediction error of V_{S30} and (b) standard deviation of V_{S30}. The color version of this figure is available only in the electronic edition.

distinct areas in the northern and northeastern parts of the basin were identified with V_{S30}-values below 180 m/s (site class E), indicating heightened susceptibility to amplification. These zones are characterized by thick, soft clay deposits in the top 30 m of the ground, with low shear-wave velocities. In contrast, central areas of the basin, with alternating layers of clay, silt, and sand, displayed V_{S30}-values between 180 and 360 m/s. Higher V_{S30}-values, ranging from 360 to 620 m/s, were observed near the eastern and southern basin margins, likely influenced by the presence of gravel and/or rock layers within the top 30 m, which significantly enhance V_S. These findings provide critical insights into spatial variations in site conditions and potential seismic hazards within the Taipei basin.

The residual map (Fig. 16b) shows residuals in the center of the basin ranging from −20 to 20 m/s, indicating close agreement between measured V_{S30}-values from the EGDT data and estimated V_{S30}-values from the CGS data. However, larger negative residuals (warm colors) appear near the basin margins, likely due to overestimation of bedrock depth in the generalized bedrock boundary (Fig. 6), which may fail to fully capture the presence of rock in those areas. As a result, the V_{S30} estimates in these zones may be underestimated due to artificially thickened soil profiles. Moreover, the marginal regions contain fewer boreholes, which can reduce the reliability of the spatial interpolation. It is also possible that engineering boreholes in these areas are more likely to be drilled in soil-dominated zones, leading to a lower likelihood of capturing shallow rock and thus further contributing to the underrepresentation of high-velocity layers in the model.

In addition, in some areas in the north and east of the basin, positive residuals (cool colors) indicate overestimated V_{S30}-values from the CGS data compared to direct EGDT measurements. These discrepancies are likely due to localized geological conditions, such as highly saturated soft sediments or unexpected low stiffness layers, which are not fully captured by the input parameters in the V_S estimation functions. Although the predicted V_{S30} at CGS borehole locations using the V_S estimation functions reflects broader average trends on physical soil parameters, the direct measurements at strong-motion stations can reveal localized effects, such as buried low-velocity layers or variations in saturation or structure, which contribute to lower observed V_{S30}. Both the positive and negative residuals emphasize the value of incorporating direct V_S data for residual correction, though Kriging with varying local means.

To further evaluate prediction reliability and variability, standard prediction error and standard deviation maps were produced (Fig. 17). The standard prediction error map (Fig. 17a) highlights regions of lower confidence in the Kriging predictions, particularly along the basin margins, where data density is sparse. Conversely, the standard deviation map (Fig. 17b) illustrates the natural variability of V_{S30}-values within localized areas. High standard deviations were observed in the southern, southeastern, and eastern parts of the basin, where diverse geological conditions, such as transitions into gravel deposits, contribute to significant changes in V_{S30} over short distances.

DISCUSSION

Influence of input parameter uncertainty on V_S and V_{S30} estimation

The reliability of the proposed V_S estimation functions is influenced by uncertainties in both of the input parameters: vertical effective stress (σ_v'), derived from groundwater level (total head), and void ratio (e), derived from laboratory tests. Groundwater level uncertainty stems from both the limitations of the model selected and seasonal fluctuations. Although the total head model was validated with an rmse of 0.52 m, this

Downloaded from http://pubs.geoscienceworld.org/ssa/bssa/article-pdf/115/5/2439/7295436/bssa-2025020.1.pdf by National Central Univ Library Serials Office user on 08 December 2025

value represents the average uncertainty in groundwater elevation used to compute vertical effective stress. In contrast, void ratio measurements are based on disturbed soil samples, which may introduce variability due to sample disturbance, incomplete saturation, or heterogeneity within the sampling interval.

To quantify how these uncertainties propagate into V_S and V_{S30}, we performed a parameter sensitivity analysis by adjusting the total head by ±3 m and the void ratio by ±0.3. The ±3 m range for total head was selected to reflect a realistic upper bound on spatial and temporal variability in groundwater level, accounting for both seasonal fluctuations and potential local deviations from the modeled values. Although the ±0.3 range for void ratio was chosen to represent the maximum expected variation due to sample disturbance and heterogeneity within the sampling interval.

Figure S3 illustrates the sensitivity of V_S and V_{S30} to changes in total head across different soil types. An increase in total head raises pore pressure and consequently reduces effective stress, leading to a consistent decrease in both V_S and V_{S30}. This effect is nonlinear, reflecting the power-law form of the effective stress term $(\frac{\sigma'_v}{P_a})^{n_a}$, with the greatest sensitivity observed in gravel due to its higher stress exponent. Despite this sensitivity, the overall change in estimated V_{S30} due to fluctuations in total head remains limited, with percent differences typically below ±5%, indicating that the model is robust to realistic variations in groundwater level.

Figure S4 shows the sensitivity of V_S and V_{S30} to changes in void ratio across different soil types. Because the void ratio increases, both V_S and V_{S30} decrease, with the greatest sensitivity observed in sand, reflecting the larger void ratio coefficient in the V_S estimation function for sand. In contrast to the nonlinear behavior seen with total head, the response to changes in void ratio is symmetric and linear, with equivalent magnitudes of change for increases and decreases. Even with a ±0.3 variation in void ratio, V_{S30} changes remained within ±4%, indicating that the influence of void ratio uncertainty on the final estimates is relatively limited.

Overall, potential fluctuations in the input parameters of the V_S estimation functions are unlikely to shift V_{S30}-values across NEHRP site class boundaries. Thus, while uncertainties in total head and void ratio do affect the estimation of V_S and V_{S30}, their influence is relatively limited in scale and does not significantly affect the reliability of the proposed method for regional seismic hazard assessment.

Influence of including shallow borehole data

To assess the influence of including extrapolated shallow V_S profiles, we compared two V_{S30} maps: one that includes shallow boreholes in the interpolation (Fig. 16c) and one that excludes them (Fig. 18a). The interpolation incorporating shallow boreholes utilized 6766 CGS boreholes, compared to 3916 boreholes when shallow boreholes were excluded, representing an ∼73% increase in data. Figure 18b highlights areas where the V_{S30} site class changes due to the exclusion of shallow borehole data, whereas Figure 18c illustrates the differences in V_{S30}-values between the two scenarios. Excluding shallow boreholes leads to site class changes over an area totaling ∼52.6 km^2, or ∼19% of the total basin area. These changes are particularly significant because variations in V_{S30} site class can have a considerable impact on seismic hazard assessments. The most prominent differences are observed in regions with a high density of shallow boreholes, notably in the northeast, southeast, and southwest of the basin. Overall, including shallow borehole data substantially improves data coverage and provides a more detailed and realistic representation of site effects. This is particularly critical in regions like the Taipei basin, where geological conditions can vary significantly over short distances.

Comparison of ordinary Kriging and Kriging with varying local means

This study employed Kriging with varying local means over ordinary Kriging to interpolate V_{S30}-values within the Taipei basin. Unlike ordinary Kriging, which assumes a constant mean across the region, Kriging with varying local means incorporates spatial variability by combining predicted V_{S30}-values with measured values and their residuals. This approach addresses potential local variations in V_{S30} that might not be captured by predicted values alone, leading to a more accurate representation of spatial variability. The final V_{S30} map produced using Kriging with varying local means is shown in Figure 16c, whereas the V_{S30} map produced using ordinary Kriging shown in Figure 19a. The differences between these approaches are significant, with areas that change site class when using ordinary Kriging instead of Kriging with varying local means totaling ∼90 km^2, or ∼33% of the basin area (Fig. 19b). Additional comparisons can be made using Figure 19c, which shows the difference in V_{S30}-values between the two methods. These changes are concentrated in the southeastern and southwestern edges of the basin, where Kriging with varying local means better captures the higher V_{S30}-values expected from the presence of shallower gravel and bedrock layers. This outcome aligns more closely with geological knowledge, providing a more realistic estimation compared to ordinary Kriging. Furthermore, the elevated V_{S30}-values in the southeastern basin identified by Kriging with varying local means are consistent with findings from previous studies (Lee and Tsai, 2008). This further validates the effectiveness of incorporating local means and residuals in the interpolation process, ensuring that variations in V_{S30} are represented accurately for seismic hazard assessments.

Advancements in V_{S30} mapping in the Taipei basin

To provide further insight into our results, we compared them to those of Lee and Tsai (2008), who used SPT-N values to produce a V_{S30} map of the Taipei basin based on drilling data from EGDT strong-motion stations collected between 2000

Downloaded from http://pubs.geoscienceworld.org/ssa/bssa/article-pdf/115/5/2439/7295436/bssa-2025020.1.pdf by National Central Univ Library Serials Office user on 08 December 2025

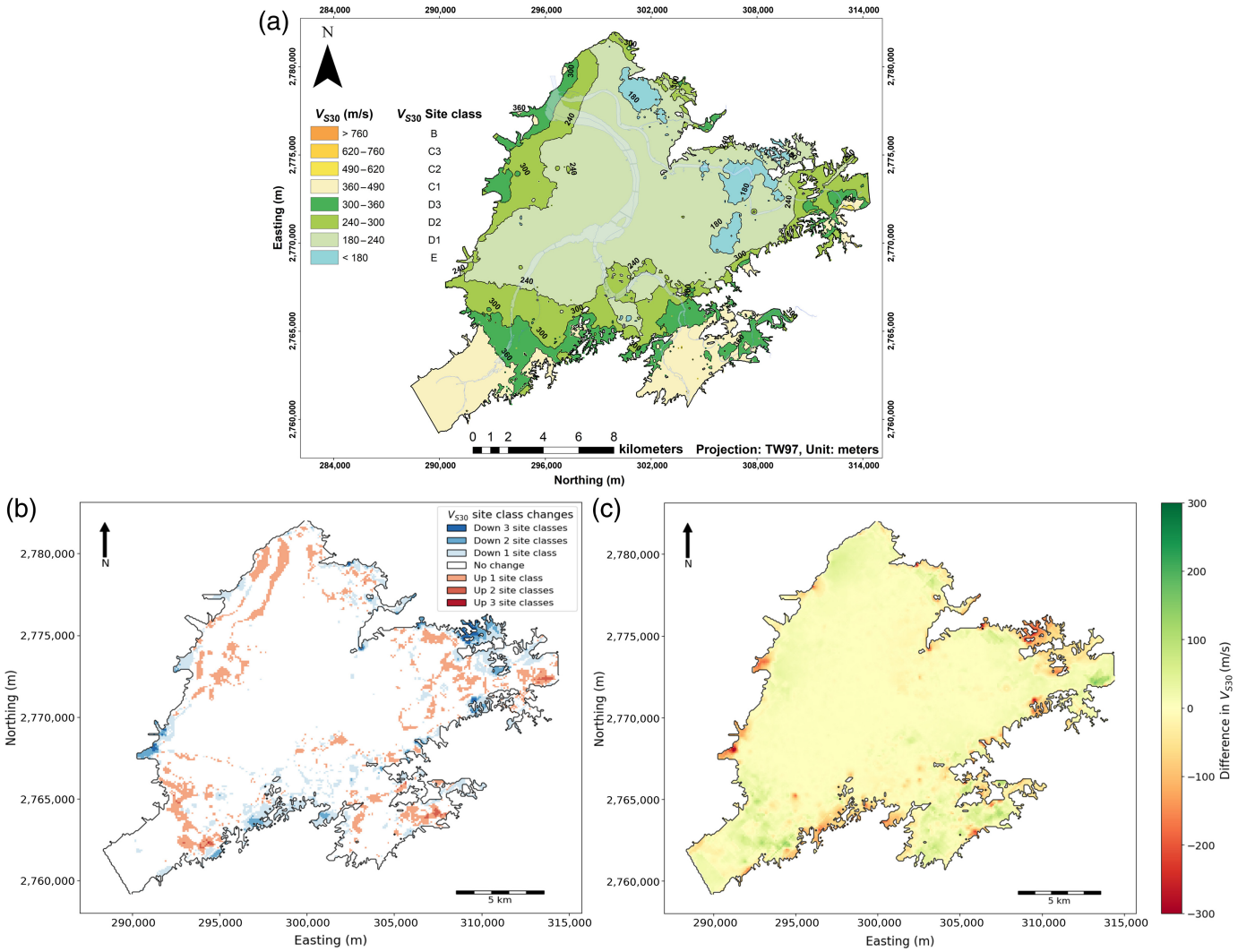

Figure 18. (a) V_{S30} map excluding shallow borehole data, (b) V_{S30} site class changes when excluding shallow borehole data, and (c) difference of V_{S30} map when excluding shallow borehole. The color version of this figure is available only in the electronic edition.

and 2004 (Fig. 20). Both studies used Kriging with varying local means to construct V_{S30} distribution maps of the Taipei basin, with measured V_{S30}-values from strong-motion stations as the primary variable and estimated V_{S30}-values from engineering boreholes as the auxiliary variable. However, our study incorporated a significantly larger dataset, resulting in greater reliability of the V_{S30} map. By comparing the V_{S30} interpolation results, several similarities and differences were observed. Both maps demonstrate similar overall trends, with most V_{S30}-values in the basin ranging from ~180 to 360 m/s. However, the map produced by Lee and Tsai (2008) shows larger areas with very high V_{S30} toward the southern and southeastern margins of the basin, a pattern not observed in our study. This difference is likely due to the limited borehole and strong-motion data available during their study, which captured general trends across the basin but lacked the resolution to identify localized variations. In addition, the use of SPT-based V_S estimation functions in Lee and Tsai (2008) may have overestimated V_S in the basin margins, where SPT refusal could have led to misrepresentation of gravel layers, resulting in artificially high V_{S30}-values. Another key difference is the distribution of low V_{S30}-values (<180 m/s). Lee and Tsai (2008) identified several small low V_{S30} areas, including three in the east and one in the north. In contrast, our results reveal a larger area with low V_{S30} in the north and only one low V_{S30} region in the east. The larger low V_{S30} area in the north is likely due to the inclusion of two additional strong-motion stations with low V_{S30} (TAP096 and TAP005) in our study, whereas differences in the east are attributed to both the substantial increase in engineering borehole data and new strong-motion station data. Finally, in the southwestern part of the basin near the Dahan and Xindian Rivers, our study shows a gradual increase in V_{S30}-values from 240–300 m/s to 300–360 m/s and subsequently to 360–490 m/s. This contrasts with the abrupt increase from 240–300 m/s to 490–620 m/s reported by Lee and Tsai (2008). This difference can also be explained by the inclusion of new

Downloaded from http://pubs.geoscienceworld.org/ssa/bssa/article-pdf/115/5/2439/7295436/bssa-2025020.1.pdf by National Central Univ Library Serials Office user on 08 December 2025

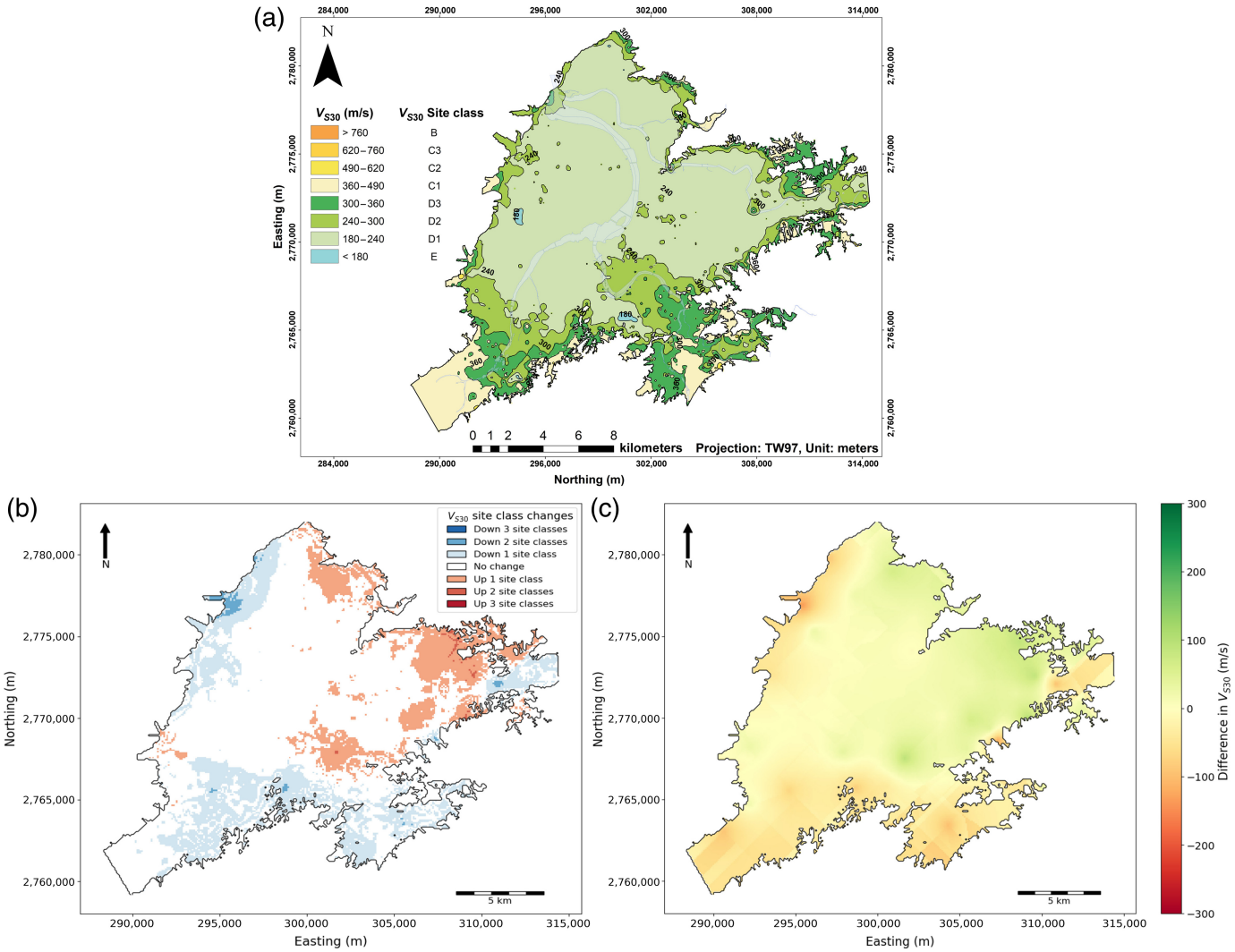

Figure 19. (a) V_{S30} map produced by ordinary Kriging, (b) V_{S30} site class changes when using ordinary Kriging, and (c) difference of V_{S30} map when using ordinary Kriging. The color version of this figure is available only in the electronic edition.

drilling data in our study, which allowed for a more comprehensive analysis of gravel layers within the top 30 m, resulting in smoother and more realistic V_{S30} gradients.

Overall, these differences highlight the advantages of the larger and more comprehensive dataset, as well as the use of V_S estimation functions based on fundamental geotechnical parameters, which provide improved spatial resolution and a more accurate representation of V_{S30} variations in the Taipei basin. However, it is also important to note that while V_{S30} is a widely used parameter for seismic site classification, it does not capture low-frequency amplification effects associated with deep sediments in the Taipei basin. Although this study does not include full seismic hazard modeling, we compared our V_{S30} results with independent observations from microtremor and earthquake recordings, including microtremor dominant frequency (f_0) data from Chen *et al.* (2022) (Fig. S5) and the seismic microzonation defined in Taiwan's building code (Fig. S6). Our V_{S30} map exhibits spatial patterns that correspond closely with f_0 and seismic microzonation, particularly near the southern and eastern basin margins, where transitions in V_{S30} align with shifts in both f_0 and seismic microzonation boundaries, supporting the reliability of the interpolation results. Within the basin, lower V_{S30}-values are generally associated with lower f_0, whereas higher V_{S30}-values outside the basin correspond to higher f_0. Nevertheless, the very low f_0-values (<0.5 Hz) observed in the central basin, classifies as zone 1 in the microzonation, indicate long-period site effects that V_{S30} alone cannot capture, likely because these effects depend on deeper basin geometry such as $Z_{1.0}$ or $Z_{2.5}$ depths (sedimentary depth from the surface to bedrocks with V_S of 1.0 and 2.5 km/s, respectively). Although this study focuses on the geotechnical and interpolation aspects of V_{S30} mapping, future research incorporating deep geophysical data and long-term seismic recordings could further clarify the relationship between V_{S30} and frequency-dependent ground-motion amplification.

Downloaded from http://pubs.geoscienceworld.org/ssa/bssa/article-pdf/115/5/2439/7295436/bssa-2025020.1.pdf by National Central Univ Library Serials Office user on 08 December 2025

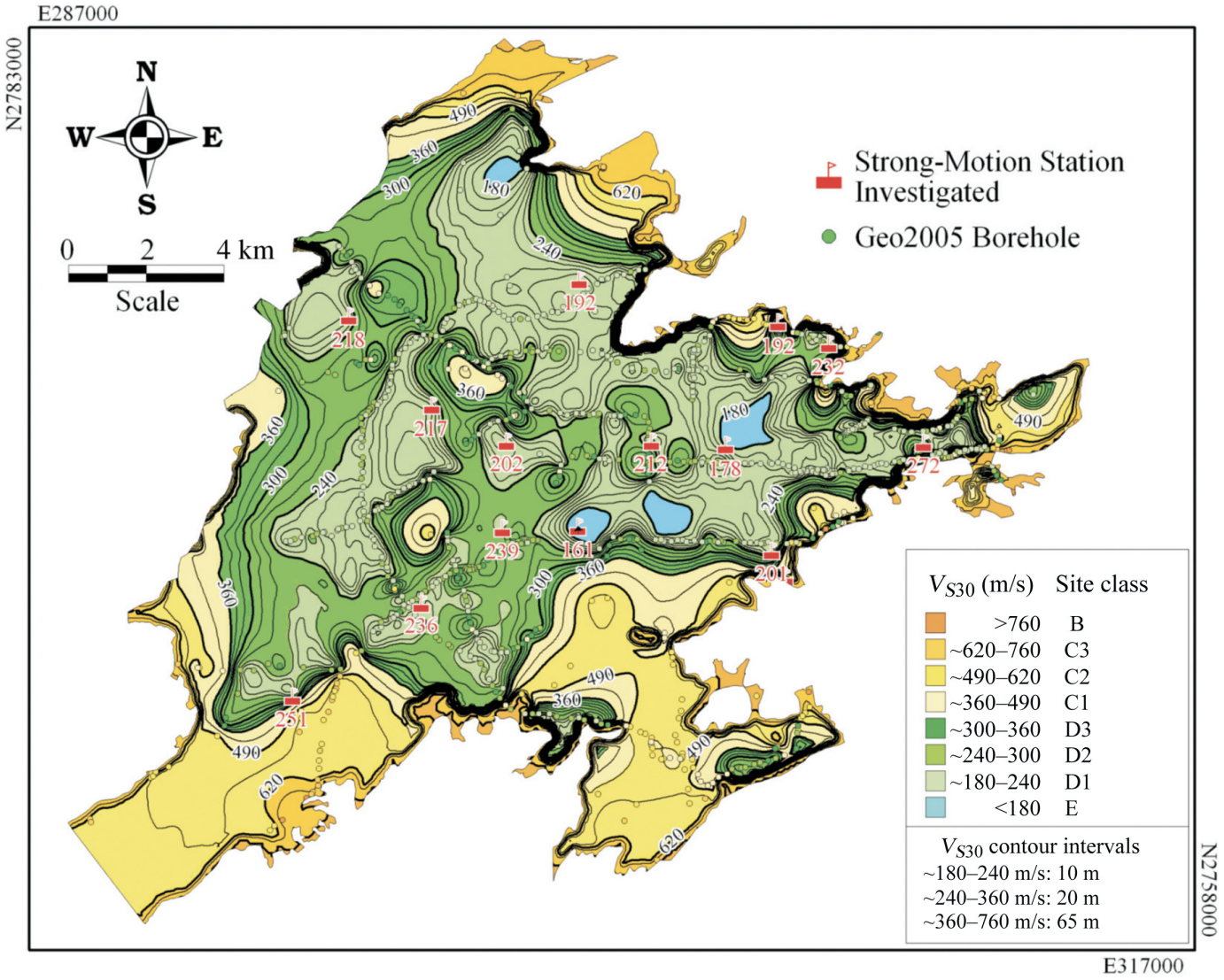

Figure 20. V_{S30} map from Lee and Tsai (2008). The color version of this figure is available only in the electronic edition.

CONCLUSION

This study utilized data from the CGS and EGDT databases to develop improved shear-wave velocity estimation functions based on the correlation between V_S, void ratio, and effective vertical stress. In addition, it compared extrapolation methods for V_S profiles less than 30-m deep and employed Kriging with varying local means for spatial interpolation to generate the V_{S30} distribution map of the Taipei basin. Key findings of this research are summarized as follows:

1. Based on the updated data from the EGDT (2000–2008) and the analysis conducted in this study, estimation functions incorporating void ratio and vertical effective stress were developed to estimate V_S for different soil types: gravel, sand, silt, and clay. These functions improved the accuracy of V_S estimation at engineering borehole locations in the Taipei basin, as evidenced by lower rmse values compared to previous studies.
2. A comparison of extrapolation methods, specifically the BCV model, CIP model, and Boore *et al.* (2011) model, was conducted. The CIP model consistently yielded the lowest rmse for extrapolating data from depths of 10–29 m to 30 m.
3. The inclusion of shallow borehole data (<30 m), extrapolated using the CIP model, increased the number of boreholes available for V_{S30} spatial interpolation by ~73%. This addition altered the V_{S30} site class for about 19% of the Taipei basin, potentially affecting seismic design parameters and contributing to more refined seismic hazard assessments.
4. The central area of the Taipei basin predominantly exhibits V_{S30}-values ranging from 180 to 300 m/s. However, isolated areas in the north and northeast show V_{S30}-values less than or equal to 180 m/s, whereas margin areas in the southeast, east, and southwest exhibit V_{S30}-values greater than or equal to 300 m/s.
5. Residual values at strong-motion stations in the central Taipei basin are generally within a range of −20 to 20 m/s.

Downloaded from http://pubs.geoscienceworld.org/ssa/bssa/article-pdf/115/5/2439/7295436/bssa-2025020.1.pdf by National Central Univ Library Serials Office user on 08 December 2025

This close agreement between measured V_{S30}-values from the EGDT strong-motion stations and predicted values from CGS boreholes underscores the accuracy of the V_{S30} interpolation in these areas.

6. The use of Kriging with varying local means provided an improved representation of local V_{S30}-values throughout the Taipei basin. ~33% of the basin experienced site class changes when using this method compared to ordinary Kriging. Higher V_{S30}-values along the basin margins were more effectively captured, emphasizing the importance of this approach for accurate site classification and seismic hazard assessments.

DATA AND RESOURCES

Measured V_S and geotechnical logging data used as the primary variable in this research was obtained from the Engineering Geological Database for the Taiwan Strong Motion Instrumentation Program (EGDT; Kuo *et al.* 2012). This data can be accessed from https://egdt.ncree.org.tw (last accessed August 2024). Borehole data for the auxiliary variables in this research were obtained from the Engineering Geological Exploration Database from the Central Geological Survey (CGS, 2002). The CGS database can be accessed through the following website: https://geotech.gsmma.gov.tw/ (last accessed August 2024). Further borehole data used by Lin (2023) to construct the contour map illustrating the elevation of the basement rock in the Taipei basin were obtained from the Hydrogeological Database from the Taiwan Ministry of Economic Affairs, which can be accessed from https://hydro.geologycloud.tw/ (last accessed October 2023). The supplemental material 1 provides additional details on groundwater models and data preprocessing. The supplemental material 2 contains the final V_{S30} map raster of the Taipei basin generated using Kriging with varying local means, that is, the result in Figure 16c. The supplemental material 3 contains the GIS files for the total head model and trend surface of the groundwater table, that is, the result shown in Figure 5.

DECLARATION OF COMPETING INTERESTS

The authors acknowledge that there are no conflicts of interest recorded.

ACKNOWLEDGMENTS

The authors express their gratitude for the data provided by the Engineering Geological Database for Taiwan Strong Motion Instrumentation Program (EGDT), supported by the National Center for Research on Earthquake Engineering (NCREE) and the Central Weather Administration (CWA; formerly the CWB) of Taiwan. The authors also extend their appreciation for the data made available by the Geological Survey and Mining Management Agency, Ministry of Economic Affairs (GSMMA; formerly CGS). This research was supported by the Ministry of Science and Technology (MOST), with the Project Number MOST 110-2123-M-008-001; the National Science and Technology Council (NSTC) with the Project Numbers NSTC 110-2123-M-008-00, NSTC 111-2123-M-008-001, NSTC 112-2123-M-008-001, NSTC 113-2123-M-008-001, and NSTC 113-2116-M-008-022. This work was also financially supported by the Earthquake Disaster & Risk Evaluation and Management Center (E-DREaM) of the Featured Areas Research Center Program within the framework of the Higher Education Sprout Project of the Ministry of Education (MOE) in Taiwan. The authors gratefully acknowledge two anonymous reviewers and the Associate Editor Fabian Bonilla's valuable comments, which have substantially enhanced the quality of this article.

REFERENCES

Ahdi, S. K., D. Y. Kwak, T. D. Ancheta, V. Contreras, T. Kishida, A. O. Kwok, S. Mazzoni, F. Ruz, and J. P. Stewart (2022). Site parameters applied in NGA-Sub database, *Earthq. Spectra* **38,** no. 1, 494–520.

Allen, T. I., and D. J. Wald (2009). On the use of high-resolution topographic data as a proxy for seismic site conditions (V_{S30}), *Bull. Seismol. Soc. Am.* **99,** no. 2A, 935–943.

Anderson, J. G., Y. Lee, Y. Zeng, and S. Day (1996). Control of strong motion by the upper 30 meters, *Bull. Seismol. Soc. Am.* **86,** 1749–1759.

Boore, D. M. (2004). Estimating V_{S30} (or NEHRP site classes) from shallow velocity models (depths <30 m), *Bull. Seismol. Soc. Am.* **94,** 591–597.

Boore, D. M., E. M. Thompson, and H. Cadet (2011). Regional correlations of V_{S30} and velocities averaged over depths less than and greater than 30 m, *Bull. Seismol. Soc. Am.* **101,** 3046–3059.

Building Seismic Safety Council (BSSC) (1995). 1994 Edition NEHRP Recommended Provisions for Seismic Regulations for New Buildings, *FEMA 222A/223A*, developed for The Federal Emergency Management Agency, Washington, D.C.

Central Geological Survey (CGS) (2002). Engineering geological database, Ministry of Economic Affairs, Taiwan, available at https://geotech.gsmma.gov.tw/ (last accessed August 2024).

Chao, S. H., C. M. Lin, C. H. Kuo, J. Y. Huang, K. L. Wen, and Y. H. Chen (2021). Implementing horizontal-to-vertical Fourier spectral ratios and spatial correlation in a ground-motion prediction equation to predict site effects, *Earthq. Spectra* **37,** no. 2, 827–856.

Chen, C. T., C. H. Kuo, C. M. Lin, J. Y. Huang, and K. L. Wen (2022). Investigation of shallow S-wave velocity structure and site response parameters in Taiwan by using high-density microtremor measurements, *Eng. Geol.* **297,** 106,498.

Craig, R. F. (2004). *Craig's Soil Mechanics*, Seventh Ed., CRC Press, Milton Park, Abingdon, Oxon, 91–133.

Dai, Z., X. Li, and C. Hou (2013). A shear-wave velocity model for V_{S30} estimation based on a conditional independence property, *Bull. Seismol. Soc. Am.* **103,** no. 6, 3354–3361.

Gutenberg, B. (1957). Effects of ground on earthquake motion, *Bull. Seismol. Soc. Am.* **47,** 221–250.

Hong, E., H. L. Poan, H. C. Liu, T. H. Lai, C. C. Huang, and L. Y. Fei (2006). The sedimentary facies and paleoenvironment analysis of the Taipei basin, *West. Pac. Earth Sci.* **6,** 59–86 (in Chinese).

Huang, T. C. (1962). The Sungshan formation in the Taipei Basin, *Mem. Geol. Soc. China.* **1,** 133–151.

Huang, M. W., J. H. Wang, K. F. Ma, C. Y. Wang, J. H. Hung, and K. L. Wen (2007). Frequency-dependent site amplifications with f ≥ 0:01 Hz evaluated from the velocity and density models in Central Taiwan, *Bull. Seismol. Soc. Am.* **97,** 624–637.

Kim, B., and T. K. Hong (2022). A national V_{S30} model for South Korea to combine nationwide dense borehole measurements with ambient seismic noise analysis, *Earth Space Sci.* **9,** no. 1, doi: 10.1029/2021EA002066.

Downloaded from http://pubs.geoscienceworld.org/ssa/bssa/article-pdf/115/5/2439/7295436/bssa-2025020.1.pdf by National Central Univ Library Serials Office user on 08 December 2025

Kuo, C. H., and N. Abrahamson (2023). Development of the Taiwan generic rock seismic velocity profile, *Seismol. Res. Lett.* **94,** 2740–2749.

Kuo, C. H., K. L. Wen, H. H. Hsieh, T. H. Chang, C. M. Lin, and C. T. Chen (2011). Evaluating empirical regression equations for V_S and estimating V_{S30} in northeastern Taiwan, *Soil Dynam. Earthq. Eng.* **31,** 431–439.

Kuo, C. H., K. L. Wen, H. H. Hsieh, C. M. Lin, T. M. Chang, and K. W. Kuo (2012). Site classification and V_{S30} estimation of free-field TSMIP stations using the logging data of EGDT, *Eng. Geol.* **129,** 68–75.

Kwok, O. L. A., J. P. Stewart, D. Y. Kwak, and O. L. Sun (2018). Taiwan-specific model for V_{S30} prediction considering between proxy correlations, *Earthq. Spectra* **34,** no. 4, 1973–1993.

Lee, C. T., and B. R. Tsai (2008). Mapping V_{S30} in Taiwan, *Terr. Atmos. Ocean. Sci.* **19,** 671–682.

Lee, C. T., T. M. Huang, C. W. Liao, and H. J. Chen (2002). The construction and application of a subsurface geologic database system: An example from the Taipei Basin, *Sino-Geotechnics* **89,** 13–26 (in Chinese).

Lin, Y.C. (2023). Mapping V_{S30} Distribution in the Taipei Basin Using Porosity, Effective Stress, and Shear Wave Velocity Relationship, *Master Thesis*, National Central University, Taiwan (in Chinese).

Park, S., and S. Elrick (1998). Predictions of shear-wave velocities in southern California using surface geology, *Bull. Seismol. Soc. Am.* **88,** 677–685.

Peng, C. H., L. S. Teng, and P. B. Yuan (1999). Facies characteristics of Taipei Basin deposits, *Central Geol. Surv. Special Publ.*, 67–99 (in Chinese).

Robertson, P. K., S. Sasitharan, J. C. Cunning, and D. C. Sego (1995). Shear-wave velocity to evaluate in-situ state of Ottawa sand, *J. Geotech. Eng.* **121,** 262–273.

Su, P. J., A. T. S. Lin, J. C. Hu, and L. S. Y. Teng (2018). Tectonic controls on the stratigraphic development of the rifted Taipei Basin: A late quaternary marine-influenced inland half graben, *Quaternary Int.* **482,** 27–45.

Teng, L. S., C. T. Lee, C. H. Peng, W. F. Chen, and C. J. Chu (2001). Origin and geological evolution of the Taipei basin, northern Taiwan, *West. Pac. Earth Sci.* **1,** 115–142.

Teng, L. S., P. B. Yuan, N. T. Yu, and C. H. Peng (2000). Sequence stratigraphy of the Taipei Basin deposits: a preliminary study, *J. Geol. Soc. China* **43,** 497–520.

Tsai, C. C., T. Kishida, and C. H. Kuo (2019). Unified correlation between SPT–N and shear wave velocity for a wide range of soil types considering strain-dependent behavior, *Soil Dynam. Earthq. Eng.* **126,** 105,783.

Wang, C. Y., Y. H. Lee, M. L. Ger, and Y. L. Chen (2004). Investigating subsurface structures and P- and S-wave velocities in the Taipei basin, *Terr. Atmos. Ocean. Sci.* **15,** 609–628.

Xie, J., X. Li, Z. Wen, L. Jia, Z. An, J. Cui, G. Lin, Q. Zhang, P. Jiang, Q. Xie, *et al.* (2022). Soil profile database and site classification for national strong-motion stations in western China, *Seismol Res. Lett.* **93,** no. 3, 1930–1942.

Xie, J, P. Zimmaro, X. Li, Z. Wen, and Y. Song (2016). V_{S30} empirical prediction relationships based on a new soil-profile database for the Beijing Plain Area, China, *Bull. Seismol. Soc. Am.* **106,** no. 6, 2843–2854.

Zhang, Y., Y. Ren, R. Wen, H. Wang, and K. Ji (2023). Regional terrain-based V_{S30} prediction models for China, *Earth Planets Space* **75,** no. 72, 1–19.

Manuscript received 11 December 2024
Published online 8 July 2025

Downloaded from http://pubs.geoscienceworld.org/ssa/bssa/article-pdf/115/5/2439/7295436/bssa-2025020.1.pdf by National Central Univ Library Serials Office user on 08 December 2025